

## Supporting Information

### **De Novo Design of Type-I Photosensitizers Agents Based on Structure-Inherent Low Triplet Energy for Hypoxia Photodynamic Therapy**

Xiao-Yun Ran,<sup>1</sup> Wen-Li Xia,<sup>1</sup> Li-Na Zhang,<sup>1</sup> Xiao-Qi Yu,<sup>1, 2</sup>, Ping Chen,<sup>3, 4</sup> Kun-Peng Xie,<sup>1</sup> Yu Zhao,<sup>1</sup> Cheng Yi,<sup>3</sup> and Kun Li<sup>1\*</sup>

<sup>1</sup>*Key Laboratory of Green Chemistry and Technology, Ministry of Education, College of Chemistry, Sichuan University, Chengdu, 610064, China.*

<sup>2</sup>*Department of Chemistry, Xihua University, Chengdu 610039, P. R. China*

<sup>3</sup>Abdominal Oncology Ward, Division of Medical Oncology, Cancer Center, West China Hospital, Sichuan University, No.37 Guoxue Alley, Chengdu, 610041, Sichuan, China.

<sup>4</sup>Department of Oncology, Chengdu Seventh People's Hospital, (Affiliated Cancer Hospital of Chengdu Medical College), Chengdu 610041, Sichuan, China

**Corresponding author: Kun Li**

E-mail: Kli@scu.edu.cn (K. Li)

## Table of Contents

SUPPLEMENTARY METHODS/SECTION.....	- 3 -
1. Materials.....	- 3 -
2. Instruments.....	- 3 -
3. Synthetic Procedure.....	- 4 -
4. Computational details.....	- 8 -
5. In vitro reactive oxygen species (ROS) detection method.....	- 8 -
6. Cyclic voltammetry and photocurrent responses measurement.....	- 9 -
7. Cell and culture conditions and Confocal Laser Scanning Microscopy Fluorescence Imaging.....	- 10 -
8. In vivo experiments.....	- 12 -
9. Statistical analysis.....	- 13 -
SUPPLEMENTARY FIGURES AND TABLES.....	- 14 -
NMR SPECTRA.....	- 38 -
REFERENCE.....	- 43 -

## SUPPLEMENTARY METHODS/SECTION

### 1. Materials

All chemicals and reagents were commercially available and used as received without further purification. The intermediate compounds were synthesized according to the previously reported procedures. 9,10-anthracenediyl-bis(methylene)dimalonic acid (ABDA), the superoxide assay kit (dihydrorhodamine 123, DHR123) for superoxide radical ( $O_2^{\cdot-}$ ) detection, singlet oxygen sensor green (SOSG), dihydroethidium (DHE) and 2'-7'-dichlorofluorescein diacetate (DCFH-DA) were purchased from Sigma-Aldrich. 3'-(4-Hydroxyphenyl) fluorescein (HPF), Alexa Fluor™ 647 conjugate, and Hoechst 33342 were purchased commercially from Molecular Probes-Invitrogen. The singlet oxygen trapping agent 2,2,6,6-tetramethyl-4-piperidine (TEMP) and free radicals trapping agent 5,5-Dimethyl-1-pyrroline N-oxide (DMPO) were purchased commercially from Adamas-beta®. For cell culture, Roswell Park Memorial Institute (RPMI) 1640, fetal bovine serum (FBS), penicillin–streptomycin solution, and Mito-Tracker Red CMXRos, Lyso-Tracker Red, Mitochondrial membrane potential assay kit, Annexin V-FITC Apoptosis Detection Kit with JC-1 and Calcein/PI Cell Viability/Cytotoxicity Assay Kit were purchased from Beyotime.

### 2. Instruments

$^1H$  and  $^{13}C$  NMR spectra were measured on a Bruker ARX 400 NMR spectrometer using  $CDCl_3$  and  $DMSO-d_6$  as solvents, and tetramethylsilane (TMS;  $\delta = 0$  ppm) was chosen as the internal reference. High-resolution mass spectra (HRMS) were obtained on a Finnigan LCQDECA mass spectrometer system operated in matrix-assisted laser desorption and ionization–time-of-flight (MALDI-TOF) mode. UV-vis absorption spectra and fluorescence emission spectra were recorded on the Duetta (HORIBA) spectrometer, and the fluorescence quantum yield were recorded on the HORIBA Fluorolog-3. CCK-8 assay was monitored by the microplate reader (SPARK, Tecan, Switzerland). The simulation was carried out with the Gaussian 09 package. Confocal laser scanning microscopic (CLSM) images of single-photo were obtained using LSM 780 (Zeiss) and analyzed using ZEN 3.4 software (Carl Zeiss).

### 3. Synthetic Procedure

Compound **FEO** was synthesized according to the previous literature<sup>[1]</sup>.

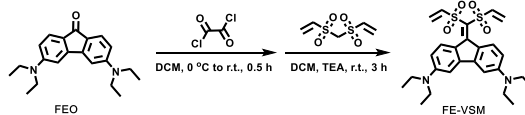


**Figure S1. Illustration of synthetic routes of FE-VSM**

The compound **FEO** (322 mg, 1 mmol, 1.0 eq) was dissolved in 15 ml dry DCM and stirred at 0 °C, and then the oxalyl chloride (30.0 eq) was dropwise to the mixture. After stirred for 30 min at 0 °C, the mixture was removed to room temperature and stirred for another 1 h, then, the mixture was concentrated under vacuum to afford the residue, which was dissolved in 20 mL dry DCM and added to the dry DCM solution of bis (vinyl sulfonyl) methane (98 mg, 0.5 eq) and triethylamine (1.1 mL, 8 eq). The mixture was stirred at room temperature for 3 h. After the reaction was completed, the solution was removed under vacuum. The residue was purified by column chromatography on silica gel (PE: DCM=1: 1) to afford **FE-VSM** (104 mg, Yield: 41.6 %). <sup>1</sup>H NMR (400 MHz, CDCl<sub>3</sub>) δ 7.68 (d, *J* = 8.9 Hz, 2H), 7.44 (d, *J* = 10.0 Hz, 1H), 7.39 (d, *J* = 10.0 Hz, 1H), 6.57 (d, *J* = 2.5 Hz, 2H), 6.49 (d, *J* = 16.7 Hz, 2H), 6.27 (dd, *J* = 9.1, 2.6 Hz, 2H), 6.08 (d, *J* = 10.0 Hz, 2H), 3.47 (q, *J* = 7.1 Hz, 8H), 1.24 (t, *J* = 7.1 Hz, 12H). <sup>13</sup>C NMR (101 MHz, CDCl<sub>3</sub>) δ 151.8, 141.2, 134.0, 125.5, 124.9, 109.4, 102.6, 44.9, 13.0. HRMS (ESI) calculated for C<sub>26</sub>H<sub>32</sub>N<sub>2</sub>O<sub>4</sub>S<sub>2</sub>Na<sup>+</sup> (*M* + Na<sup>+</sup>) 523.1696, observed 523.1715.

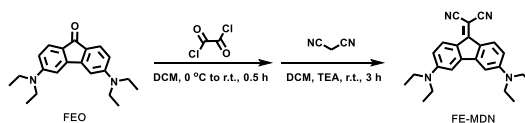


**Figure S2. Illustration of synthetic routes of FE-MDN**

The compound **FEO** (322 mg, 1 mmol, 1.0 eq) was dissolved in 15 ml dry DCM and stirred at 0 °C, and then the oxalyl chloride (30.0 eq) was dropwise to the mixture. After stirred for 30 min at 0 °C, the mixture was removed to room temperature and stirred for another 1 h, then, the mixture was concentrated under vacuum to afford the residue, which was dissolved in 20 mL dry DCM and added to the dry DCM solution of malononitrile (66 mg, 1 eq) and triethylamine (1.1 mL, 8 eq). The mixture was stirred at room temperature for 3 h. After the reaction was completed, the solution was removed under vacuum. The residue was purified by column chromatography on silica gel (PE:

DCM=1: 1) to afford FE-MDN (230 mg, Yield: 62.0%).  $^1\text{H}$  NMR (400 MHz,  $\text{CDCl}_3$ )  $\delta$  8.10 (d,  $J = 8.9$  Hz, 2H), 6.72 (d,  $J = 2.5$  Hz, 2H), 6.39 (dd,  $J = 9.0, 2.5$  Hz, 2H), 3.50 (q,  $J = 7.1$  Hz, 8H), 1.26 (t,  $J = 7.1$  Hz, 12H).  $^{13}\text{C}$  NMR (101 MHz,  $\text{CDCl}_3$ )  $^{13}\text{C}$  NMR (101 MHz, Chloroform-*d*)  $\delta$  160.03, 151.68, 144.51, 128.35, 122.98, 116.57, 109.86, 102.77, 44.89, 12.87. HRMS (ESI) calculated for  $\text{C}_{24}\text{H}_{27}\text{N}_4^+$  ( $\text{M}^+ + \text{H}^+$ ) 371.2230, observed 371.2236.

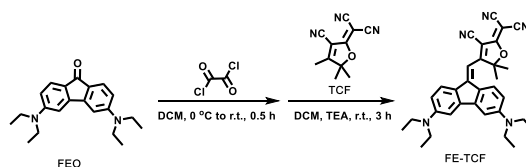


**Figure S3. Illustration of synthetic routes of FE-TCF**

The compound FEO (322 mg, 1 mmol, 1.0 eq) was dissolved in 15 ml dry DCM and stirred at 0 °C, and then the oxalyl chloride (30.0 eq) was dropwised to the mixture. After stirred for 30 min at 0 °C, the mixture was removed to room temperature and stirred for another 1 h, then, the mixture was concentrated under vacuum to afford the residue, which was dissolved in 20 mL dry DCM and added to the dry DCM solution of TCF (100 mg, 0.5 eq) and triethylamine (1.1 mL, 8 eq). The mixture was stirred at room temperature for 3 h. After the reaction was completed, the solution was removed under vacuum. The residue was purified by column chromatography on silica gel (DCM) to afford FE-TCF (126 mg, Yield: 51.1%).  $^1\text{H}$  NMR (400 MHz,  $\text{CDCl}_3$ )  $\delta$  7.36 (d,  $J = 8.6$  Hz, 2H), 6.75 (d,  $J = 2.4$  Hz, 2H), 6.45 (d,  $J = 7.3$  Hz, 2H), 6.10 (s, 1H), 3.50 (q,  $J = 7.1$  Hz, 8H), 1.69 (s, 6H), 1.26 (t,  $J = 7.0$  Hz, 12H).  $^{13}\text{C}$  NMR (101 MHz,  $\text{CDCl}_3$ )  $\delta$  175.7, 155.5, 151.2, 113.1, 111.9, 109.7, 103.3, 98.3, 97.5, 44.9, 26.2, 12.9. HRMS (ESI) calculated for  $\text{C}_{32}\text{H}_{34}\text{N}_5\text{O}^+$  ( $\text{M}^+ + \text{H}^+$ ) 504.2758, observed 504.2758.

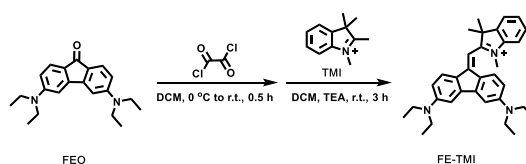


**Figure S4. Illustration of synthetic routes of FE-TMI**

The compound FEO (322 mg, 1 mmol, 1.0 eq) was dissolved in 15 ml dry DCM and stirred at 0 °C, and then the oxalyl chloride (30.0 eq) was dropwised to the mixture. After stirred for 30 min at 0 °C, the mixture was removed to room temperature and stirred for another 1 h, then, the mixture was concentrated under vacuum to afford the residue, which was dissolved in 20 mL dry

DCM and added to the dry DCM solution of TMI (127 mg, 0.5 eq) and triethylamine (1.1 mL, 8 eq). The mixture was stirred at room temperature for 3 h. After the reaction was completed, the solution was removed under vacuum. The residue was purified by column chromatography on silica gel (DCM: MeOH=10: 1). Then FE-TMI and KBr were dissolved in acetone and stirred overnight at room temperature. The mixture was extracted with dichloromethane and water, and then the organic phase was evaporated under a vacuum to afford pure FE-TMI (115 mg, Yield: 41.2%). <sup>1</sup>H NMR (400 MHz, CDCl<sub>3</sub>) δ 7.77 (d, *J* = 8.0 Hz, 1H), 7.58 (td, *J* = 7.7, 1.5 Hz, 1H), 7.52 – 7.43 (m, 2H), 7.15 (d, *J* = 8.8 Hz, 2H), 6.89 (d, *J* = 2.4 Hz, 2H), 6.46 (dd, *J* = 8.8, 2.4 Hz, 2H), 6.40 (s, 1H), 3.84 (s, 3H), 3.55 (q, *J* = 7.1 Hz, 8H), 1.67 (s, 6H), 1.28 (t, *J* = 7.1 Hz, 12H). <sup>13</sup>C NMR (101 MHz, CDCl<sub>3</sub>) δ 159.0, 152.2, 145.4, 143.0, 140.4, 129.6, 128.1, 127.4, 125.2, 122.6, 114.5, 110.3, 104.4, 92.1, 52.4, 45.2, 38.8, 26.0, 13.0. HRMS (ESI) calculated for C<sub>33</sub>H<sub>40</sub>N<sub>3</sub><sup>+</sup> (M<sup>+</sup>) 478.3217, observed 478.3214.

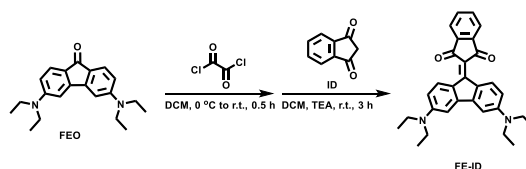


**Figure S5. Illustration of synthetic routes of FE-ID**

The compound FEO (322 mg, 1 mmol, 1.0 eq) was dissolved in 15 ml dry DCM and stirred at 0 °C, and then the oxalyl chloride (30.0 eq) was dropwisely added to the mixture. After stirred for 30 min at 0 °C, the mixture was removed to room temperature and stirred for another 1 h, then, the mixture was concentrated under vacuum to afford the residue, which was dissolved in 20 mL dry DCM and added to the dry DCM solution of ID (73 mg, 0.5 eq) and triethylamine (1.1 mL, 8 eq). The mixture was stirred at room temperature for 3 h. After the reaction was completed, the solution was removed under vacuum. The residue was purified by column chromatography on silica gel (PE: DCM=1: 1) to afford pure FE-ID (72.6 mg, Yield: 32.2%). <sup>1</sup>H NMR (400 MHz, CDCl<sub>3</sub>) δ 8.38 (d, *J* = 9.2 Hz, 2H), 7.81 (dd, *J* = 5.4, 3.1 Hz, 2H), 7.62 (dd, *J* = 5.5, 3.0 Hz, 2H), 6.64 (s, 2H), 6.32 (d, *J* = 9.2 Hz, 2H), 3.47 (q, *J* = 7.1 Hz, 8H), 1.24 (d, *J* = 7.2 Hz, 12H).

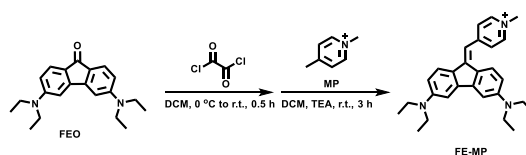


**Figure S6. Illustration of synthetic routes of FE-MP**

The compound FEO (322 mg, 1 mmol, 1.0 eq) was dissolved in 15 ml dry DCM and stirred at 0 °C, and then the oxalyl chloride (30.0 eq) was dropwised to the mixture. After stirred for 30 min at 0 °C, the mixture was removed to room temperature and stirred for another 1 h, then, the mixture was concentrated under vacuum to afford the residue, which was dissolved in 20 mL dry DCM and added to the dry DCM solution of MP (96.5 mg, 0.5 eq) and triethylamine (1.1 mL, 8 eq). The mixture was stirred at room temperature for 3 h. After the reaction was completed, the solution was removed under vacuum. The residue was purified by column chromatography on silica gel (DCM: MeOH=10: 1). Then FE-MP and KBr were dissolved in acetone and stirred overnight at room temperature. The mixture was extracted with dichloromethane and water, and then the organic phase was evaporated under a vacuum to afford pure FE-MP (63.5 mg, Yield: 25.8%). <sup>1</sup>H NMR (400 MHz, CDCl<sub>3</sub>) δ 8.70 (d, *J* = 6.4 Hz, 2H), 7.92 (d, *J* = 6.4 Hz, 2H), 7.70 (d, *J* = 8.8 Hz, 1H), 7.44 (d, *J* = 9.0 Hz, 1H), 6.78 (s, 2H), 6.67 (s, 1H), 6.51 (d, *J* = 8.2 Hz, 1H), 6.40 (d, *J* = 10.0 Hz, 1H), 4.46 (s, 3H), 3.47 (d, *J* = 7.2 Hz, 8H), 1.24 (t, *J* = 6.6 Hz, 12H).

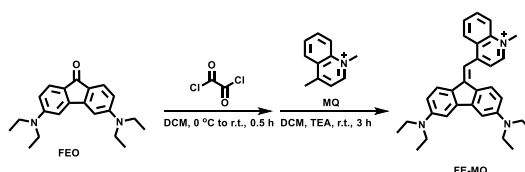


**Figure S7. Illustration of synthetic routes of FE-MQ**

The compound FEO (322 mg, 1 mmol, 1.0 eq) was dissolved in 15 ml dry DCM and stirred at 0 °C, and then the oxalyl chloride (30.0 eq) was dropwised to the mixture. After stirred for 30 min at 0 °C, the mixture was removed to room temperature and stirred for another 1 h, then, the mixture was concentrated under vacuum to afford the residue, which was dissolved in 20 mL dry DCM and added to the dry DCM solution of MQ (119 mg, 0.5 eq) and triethylamine (1.1 mL, 8 eq). The mixture was stirred at room temperature for 3 h. After the reaction was completed, the solution was removed under vacuum. The residue was purified by column chromatography on silica gel (DCM: MeOH=10: 1). Then FE-MQ and KBr were dissolved in acetone and stirred overnight at room temperature. The mixture was extracted with dichloromethane and water, and then the organic phase was evaporated under a vacuum to afford pure FE-MQ (82.7 mg, Yield: 31.3%). <sup>1</sup>H NMR (400 MHz, CDCl<sub>3</sub>) δ 9.75 (d, *J* = 6.4 Hz, 1H), 8.49 (d, *J* = 8.4 Hz, 1H), 8.26 (d, *J* = 6.4 Hz, 1H), 8.15 (d, *J* = 8.8 Hz, 1H), 8.08 (t, *J* = 8.5 Hz, 1H), 7.83 (t, *J* = 7.7 Hz, 1H), 7.57 (d, *J* = 8.7 Hz, 2H), 7.19 (s, 1H), 6.81 (d, *J* = 14.3 Hz, 2H), 6.56 (d, *J* = 8.6 Hz, 1H), 6.37 (d, *J* = 8.9 Hz, 1H), 4.74 (s, 3H), 3.49 (dq, *J* = 14.2, 6.9, 6.4 Hz, 8H), 1.26 (dt, *J* = 13.9, 7.0 Hz, 12H).

#### 4. Computational details<sup>[2]</sup>

Theoretical calculation details. CAM-B3LYP/def2SVP calculations were carried out using Gaussian 09 program. Density functional theory (DFT) and time-dependent DFT (TD-DFT) were employed to acquire the energy levels of both singlet excited states and investigate the energy levels of both singlet excited states and reactive oxygen species production mechanism of all compounds (ORCA, Program Version 5.0.3). All structural optimizations in the ground and excited states were performed using CAM-B3LYP functional and Def2SVP basis set. Solvation effects in water were taken into account using the SMD model.

#### 5. In vitro reactive oxygen species (ROS) detection method<sup>[3,4]</sup>

##### 5.1 The total ROS detection

According to the previous reference, the total ROS detection experiments commonly used ROS chemical indicator 2',7'-dichlorofluorescein diacetate (DCFH-DA) was hydrolyzed into 2',7'-dichlorofluorescein (DCFH) to afford the final concentration at 40  $\mu\text{M}$ . In brief, 250  $\mu\text{L}$  of DCFH stock solution (50  $\mu\text{M}$ ) was added to 0.75 mL of FE-VSM, FE-MDN, FE-TCF, FE-TMI or Ce6 suspension with the final concentration of 10  $\mu\text{M}$ . The PL spectra of DCFH were observed with excitation wavelength at 488 nm and emission spectra region was collected from 500 to 600 nm at green light irradiation time (50  $\text{mW cm}^{-2}$ ). The emission intensity at 525 nm was analyzed to demonstrate the generation rate of total ROS.

##### 5.2 $^1\text{O}_2$ detection

9,10-Anthracenediyl-bis(methylene)dimalonic acid (ABDA) was employed as the  $^1\text{O}_2$  generation indicator. In the measurements, 20  $\mu\text{L}$  of ABDA stock solution (10 mM in dimethylsulfoxide) was added to 2 mL of FE-VSM, FE-MDN, FE-TCF, FE-TMI, or Ce6 suspension (10  $\mu\text{M}$ ) with green light irradiation (50  $\text{mW cm}^{-2}$ ). The absorption spectra of ABDA from 350 to 450 nm were recorded at various irradiation time (0-5 min), and the decomposition rate ( $A/A_0$ ) was determined by the absorbance signal decrease of ABDA at 378 nm.

##### 5.3 $\text{O}_2^{\cdot-}$ detection



Dihydrorhodamine123 (DHR123) was employed as the  $O_2^{\bullet-}$  generation indicator. In the experiments, 10  $\mu$ L of DHR123 stock solution (5 mM in dimethylsulfoxide) was added to 2 mL of FE-VSM, FE-MDN, FE-TCF or FE-TMI suspension (10  $\mu$ M). Upon the green light irradiation (50  $mW\ cm^{-2}$ ), the PL spectra variation of DHR123 from 500 to 620 nm were monitored at various irradiation time with the excitation wavelength at 495 nm, and the fluorescence intensity at 526 nm was obtained to determine the generation rate of  $O_2^{\bullet-}$ .

#### **5.4 $\bullet$ OH detection**

$\bullet$ OH detection in aqueous solution Hydroxyphenyl fluorescein (HPF) was employed as the  $\bullet$ OH generation indicator. In the detection experiments, 2  $\mu$ L of HPF stock solution (10 mM N-dimethylformamide) was added to 2 mL of FE-VSM, FE-MDN, FE-TCF or FE-TMI suspension (10  $\mu$ M). The resultant fluorescence signal variation of HPF from 500 to 600 nm were detected at different time intervals with the excitation wavelength at 490 nm after the green light irradiation (50  $mW\ cm^{-2}$ ), and the fluorescence intensity at 515 nm was adopted to determine the generation rate of  $\bullet$ OH.

#### **5.5 EPR analysis**

EPR analysis was performed to confirm the generation of  $O_2^{\bullet-}$  utilizing DMPO as spin trap agent. The detecting samples containing DMPO (80 mM) and FE-VSM or FE-TMI suspension (0.5 mg/mL) in MeCN were added quantitatively into quartz capillaries. Then, the spectra of spin were obtained before and after the corresponding solutions were irradiated by green light (50  $mW\ cm^{-2}$ ) for 5 min. The generation of  $\bullet$ OH was confirmed in  $H_2O$  by EPR analysis with the similar experiment conditions. EPR spectra for the detection of  $^1O_2$  using TEMP (water) as a spin trapper. The reaction mixture was containing TEMP (50 mM)/FE-VSM (0.5 mg/mL) or TEMP (50 mM)/ FE-TMI (0.5 mg/mL) upon green light irradiation for 5 min (50  $mW\ cm^{-2}$ ).

## **6. Cyclic voltammetry and photocurrent responses measurement**

### **6.1 Cyclic voltammetry measurement**

Cyclic voltammograms experiment was conducted by using a three-electrode system. A platinum-carbon compound electrode was used as the working electrode, the Pt wire electrode and the Ag/Ag<sup>+</sup> electrode were used as the auxiliary electrode and reference electrode, respectively. The

measurement was conducted in water containing 0.1 M Phosphate Buffered Saline hexafluorophosphate (PBS). The scan rate was optimized as 100 mV/s. Fc/Fc<sup>+</sup> was used as an external reference.

## **6.2 Photocurrent responses measurement**

The photocurrent responses experiment was conducted by using a three-electrode system. A carbon paper electrode attached FE-VSM or FE-TMI was used as the working electrode, the platinum electrode and the Ag/AgCl electrode was used as the counter electrode and reference electrode, respectively. The measurement was conducted in 0.1 M sodium sulfate buffer and irradiated by a white LED light (40 mW/cm<sup>2</sup>) with an interval of 25 s.

## **7. Cell and culture conditions and Confocal Laser Scanning Microscopy Fluorescence Imaging.**

### **7.1 Cell culture**

4T-1 cells were cultured in Roswell Park Memorial Institute RPMI 1640 medium (Gibco) supplemented with 10% fetal calf serum (FBS) and 1% antibiotic solution (0.1 mg mL<sup>-1</sup>) at 37°C in 95% air with 5% CO<sub>2</sub>. 1 × 10<sup>5</sup> 4T-1 cells were firstly plated onto 35 mm confocal dishes and incubated for 24 h for specific fluorescence images.

### **7.2 Cell viability assay**

The cell growth inhibition of FE-VSM, and FE-TMI for the 4T-1 cell lines was determined using the standard CCK-8 cell viability assay kit (Beyotime). Briefly, ca. 1 × 10<sup>4</sup> cells were first seeded in 96 well plates and then incubated for 24 h with either FE-VSM, and FE-TMI followed by washing with serum-free medium. The cells were then incubated with the CCK-8 reagent for 1 h before determining the absorbance at 450 nm using a Tecan microplate reader.

### **7.3 Cell imaging**

A total of ca. 5 × 10<sup>5</sup> 4T-1 cells were seeded in glass bottom dishes and cultured overnight at 37°C. The cells were the incubated with 2 μM FE-VSM, FE-MQ, FE-TCF and FE-TMI for 30 min and followed by incubation for 30 min with 2 μM 2',7'-dichlorofluorescein diacetate (DCFH-DA)

used as an ROS probe. The cells were then washed with PBS and irradiated using a white LED light source for 20 min at a power density of 50 mW/cm<sup>2</sup>. The fluorescence (if any) was recorded immediately using a confocal laser scanning microscope (CLSM) with an excitation wavelength of 488 nm. The emission was collected from 500 nm to 550 nm

#### **7.4 Intracellular total ROS detection**

A total of ca.  $5 \times 10^5$  4T-1 cells were seeded in 35 mm confocal dishes and incubated for 24 hours under a normoxic (21% O<sub>2</sub>) or hypoxia (< 1% O<sub>2</sub>) environment and cultured overnight at 37°C. The cells were then incubated with 2 μM FE-TMI and 5 μM 2',7'-dichlorofluorescein diacetate (DCFH-DA) used as an ROS probe. The cells were then washed with PBS and irradiated using a green LED light source for 5 min at a power density of 50 mW/cm<sup>2</sup>. The fluorescence was recorded immediately using a confocal laser scanning microscope (CLSM) with an excitation wavelength of 488 nm. The emission was collected from 500 nm to 550 nm. The measurement of intracellular ROS was carried out using a commercially Reactive Oxygen Species Assay Kit.

#### **7.5 •OH generation in living cells**

4T-1 cells were seeded in 35 mm confocal dishes and incubated for 24 hours under a normoxic (21% O<sub>2</sub>) environment. Specifically, the 4T-1 cells were incubated with 2 μM FE-TMI at 37 °C for 30 min and then washed with PBS three times. The culture medium was replaced with RPMI 1640 containing 2 μM HPF (hydroxyphenyl fluorescein) and incubated for 30 min. After that, the RPMI 1640 was removed and washed three times with PBS buffer. The cells were then subjected to the photosensitization experiment with a green LED irradiation (50 mW/cm<sup>2</sup>) for 5 min. Fluorescence images of HPF and staining on the cells were promptly captured by laser scanning confocal microscopy (CarlZeiss, LSM780).

#### **7.6 O<sub>2</sub><sup>-</sup> generation in living cells**

A total of ca.  $5 \times 10^5$  4T-1 cells were seeded in 35 mm confocal dishes and incubated for 24 hours under a normoxic (21% O<sub>2</sub>) or hypoxia (< 1%) environment and cultured overnight at 37°C. Specifically, the 4T-1 cells were incubated with 2 μM FE-TMI at 37 °C for 30 min and then washed three times with PBS buffer. The culture medium was replaced with RPMI 1640 containing

10  $\mu\text{M}$  DHE and incubated for another 30 min. After that, the RPMI 1640 was removed and washed with PBS buffer three times. The cells were then subjected to the photosensitization experiment with a green LED irradiation ( $50 \text{ mW}/\text{cm}^2$ ) for 5 min. The fluorescent images of DHE, staining on the cells were promptly captured by laser scanning confocal microscopy (CarlZeiss, LSM780).

### **7.7 $^1\text{O}_2$ generation in living cells**

4T-1 cells were seeded in 35 mm confocal dishes and incubated for 24 h. Specifically, the 4T-1 cells were incubated with  $2 \mu\text{M}$  FE-TMI at  $37^\circ\text{C}$  for 30 min and then washed three times with PBS buffer. The culture medium was replaced with RPMI 1640 containing  $1 \mu\text{M}$  singlet oxygen sensor green (SOSR) and incubated for another 30 min. After that, the RPMI 1640 was removed and washed with PBS buffer three times. The cells were then subjected to the photosensitization experiment with a green LED irradiation ( $50 \text{ mW}/\text{cm}^2$ ) for 5 min. The fluorescent images of SOSR, staining on the cells were promptly captured by laser scanning confocal microscopy (CarlZeiss, LSM780).

### **7.8 Calcein AM/PI staining of 4T-1 cells in PDT experiments**

4T-1 cells were seeded on 35 mm confocal dishes and incubated for 24 hours. The medium was then replaced with a fresh culture medium containing different concentrations of  $2 \mu\text{M}$  FE-TMI and incubated for 30 min. Then, the culture medium was replaced with fresh RPMI 1640 containing  $5 \mu\text{M}$  Calcein AM (Calcein acetoxymethyl ester) and  $5 \mu\text{M}$  propidium iodide (PI). After further incubation for 20 min, the Calcein AM and PI solution was removed and washed with PBS buffer three times. After that, the cells were irradiated with a green LED light ( $50 \text{ mW}/\text{cm}^2$ ) for 5 min. The fluorescent images of Calcein AM and PI, staining on the cells, were promptly captured by laser scanning confocal microscopy (CarlZeiss, LSM780).

## **8. In vivo experiments**

### **8.1 In vivo imaging**

Tumor imaging in vivo was studied with subcutaneous 4T-1 tumor model in the immunocompetent BALB/c mice. The tumor-bearing mice were intravenously injected of FE-TMI

(2.0mg/kg). Then, the fluorescence was recorded at different time points (0, 0.5, 1, 2, 3, 5, 7 hours) with an IVIS Spectrum imaging system.

## **8.2 In vivo antitumor activity**

To investigate the antitumor effect of the FE-TMI, Balb/c mice were subcutaneously injected with  $1 \times 10^6$  4T-1 cells. When the tumor volume achieved approximately 80-120 mm<sup>3</sup>, tumor bearing mice were randomly divided into 4 groups (each group included 4 mice): 1) PBS; 2) PBS+Light; 3) FE-TMI; 4) FE-TMI+Light. 50  $\mu$ L PBS or 50  $\mu$ L FE-TMI (2.0 mg/kg) were directly injected into tumors. Then, tumor sites were exposed to green light radiation (50 mW/cm<sup>2</sup>) for 5 min after 2 h post injection. After various treatments, the body weight and tumor volume were recorded every 2 days. Two weeks of treatment, all the mice were sacrificed. Five main organs (heart, liver, spleen, lung, and kidney) and tumors of all mice were harvested, washed with PBS, and fixed with paraformaldehyde for histology analysis. And the tumor tissues were weighed, and fixed in 4% neutral buffered formalin, processed routinely into paraffin, and sectioned at 4  $\mu$ m. Then the sections were stained with hematoxylin-eosin (H&E) staining and Terminal deoxynucleotidyl transferase-mediated deoxyuridinetriphosphate nick end labeling (TUNEL) and finally examined by using an optical microscope (BX51, Olympus, Japan). All animal procedures were conducted in accordance with Approval No. 20230220037 of the West China Hospital of Sichuan University and the Animal Ethics Committee on the protection of animals used in research.

## **9. Statistical analysis**

All the data were shown as the average value  $\pm$  SD. Unless stated otherwise, the sample size was three (n = 3). The significance of the difference was decided through one-way analysis of variance by software GraphPad Prism (ns p > 0.05, \*p < 0.05, \*\*p < 0.01, \*\*\*p < 0.001, \*\*\*\*p < 0.0001).

## SUPPLEMENTARY FIGURES AND TABLES

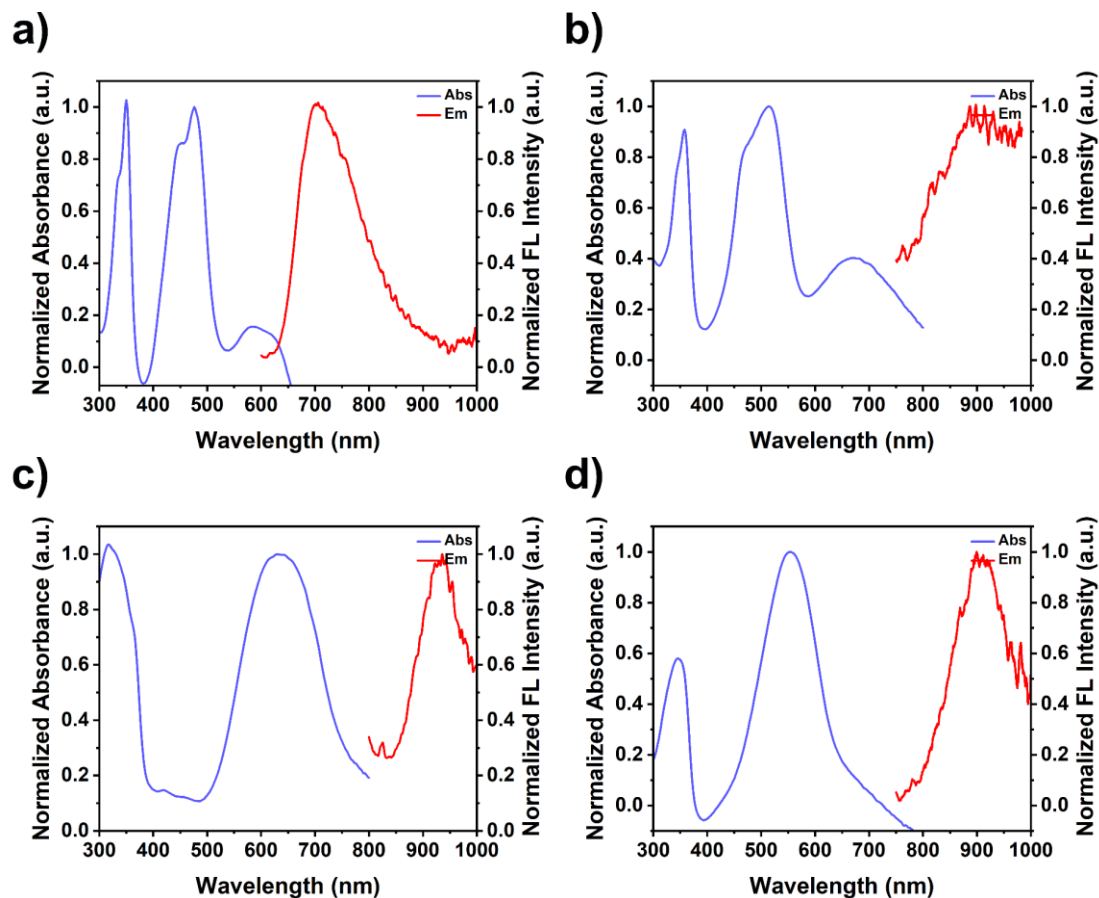


**Figure S8.** Normalized absorption and emission spectra of (a) FE-MDN, (b) FE-VSM, (c) FE-TCF and (d) FE-TMI in PBS ( $c = 10 \mu\text{M}$ , Slite = 20 nm).

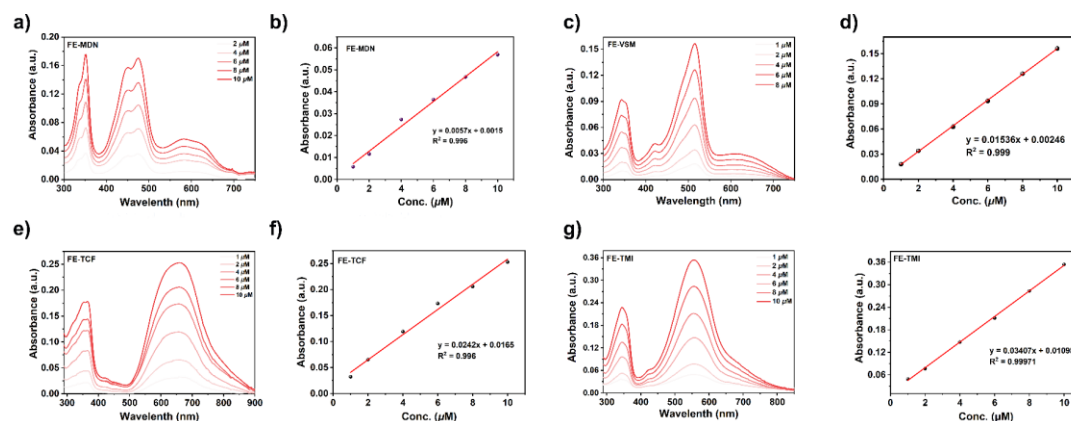


**Figure S9.** Absorption spectrum of (a) FE-MDN, (c) FE-VSM, (e) FE-TCF and (g) FE-TMI in PBS with different concentrations (0 to  $10 \mu\text{M}$ ), the maximum absorption value of (b) FE-MDN, (d) FE-VSM, (f) FE-TCF and (h) FE-TMI in PBS increase linearly with concentration from 2 to  $10 \times 10^{-6}$  M.

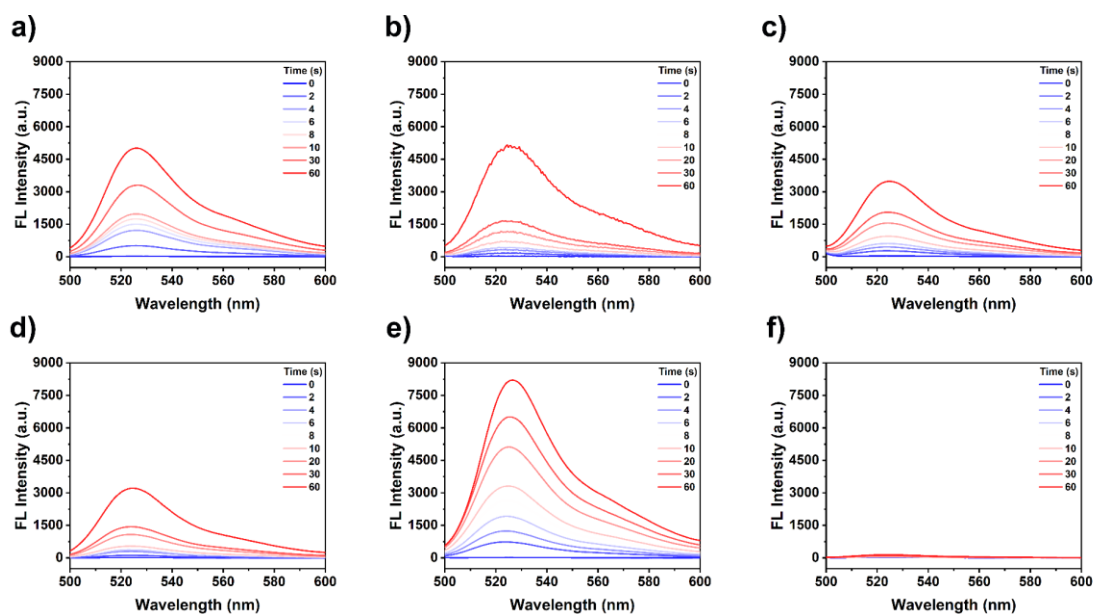


**Figure S10.** The fluorescence spectrum of DCFH-DA with (a) Ce6 (10  $\mu$ M), (b) FE-MDN (10  $\mu$ M), (c) FE-VSM (10  $\mu$ M), (d) FE-TCF (10  $\mu$ M), (e) FE-TMI (10  $\mu$ M) and (f) Control (blank) in PBS solution upon the green LED irradiation (50 mW/cm<sup>2</sup>) for 60s.

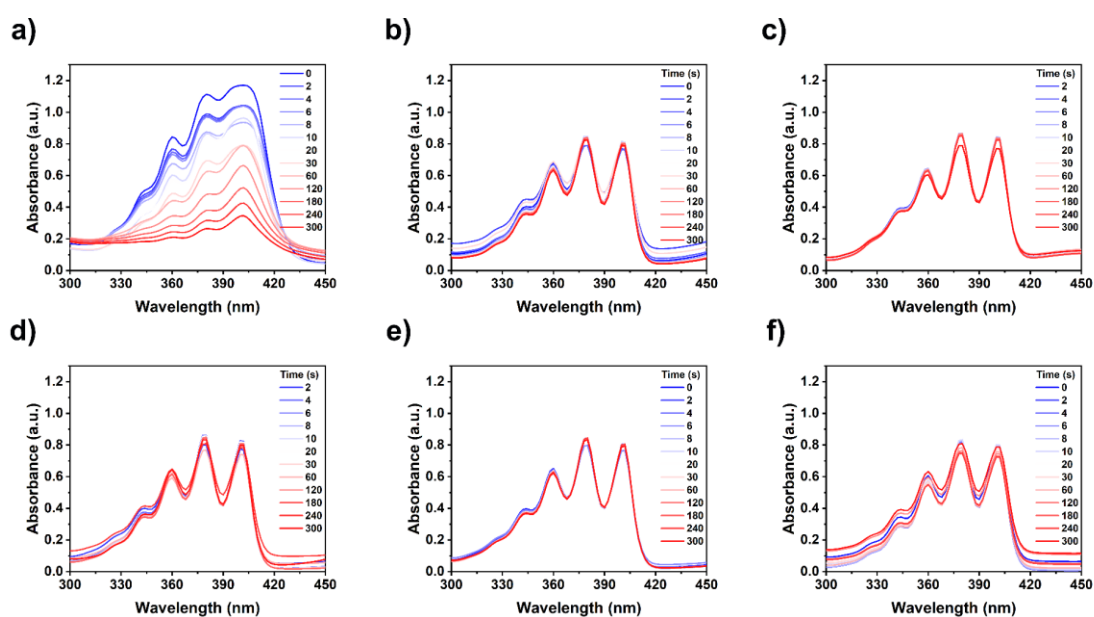


**Figure S11.** The absorbance spectrum of ABDA with (a) Ce6 (10  $\mu$ M), (b) FE-MDN (10  $\mu$ M), (c) FE-VSM (10  $\mu$ M), (d) FE-TCF (10  $\mu$ M), (e) FE-TMI (10  $\mu$ M) and (f) Control (blank) in PBS solution upon the green LED irradiation (50 mW/cm<sup>2</sup>) for 300s.

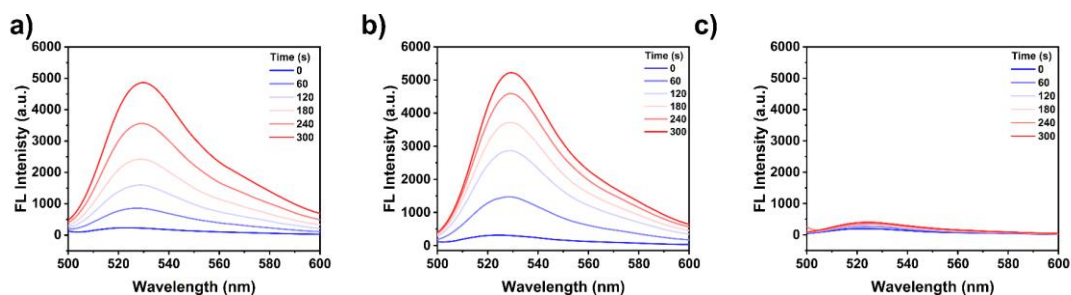


**Figure S12.** The fluorescence spectrum of DHR123 with (a) FE-VSM (10  $\mu$ M), (b) FE-TMI (10  $\mu$ M) (c) Blank in PBS solution upon the green LED irradiation (50  $\text{mW}/\text{cm}^2$ ) for 300s.

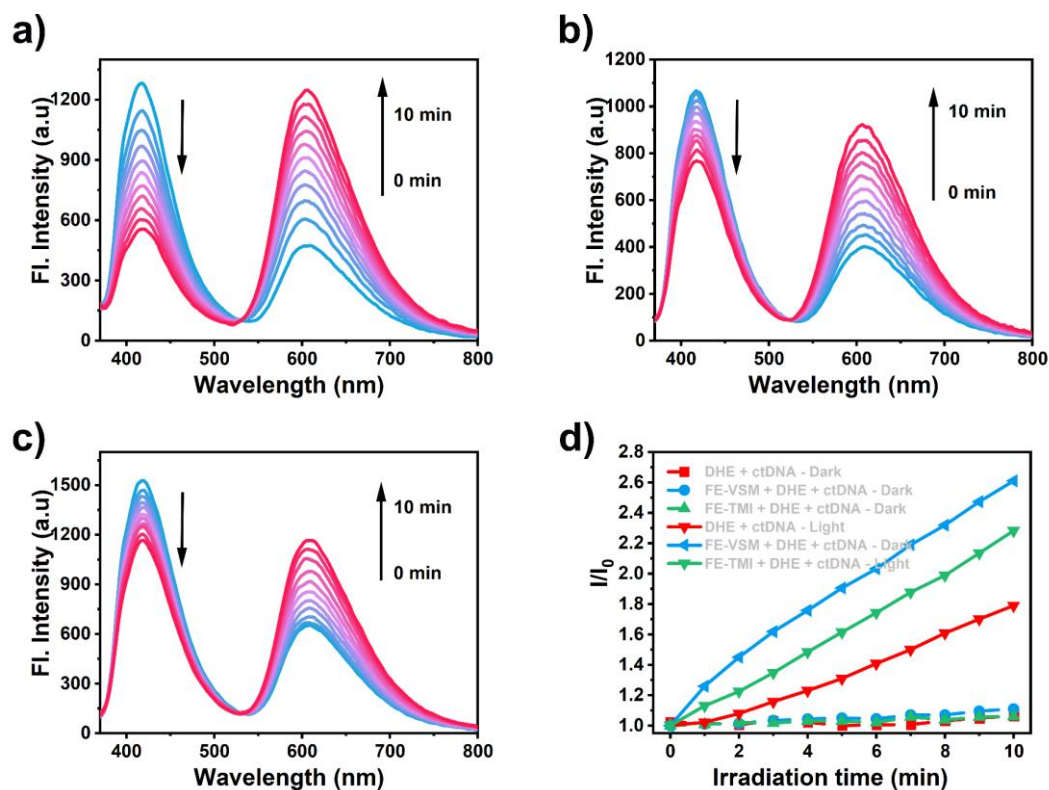


**Figure S13.** The fluorescence spectrum of DHE with (a) FE-VSM (10  $\mu$ M), (b) FE-TMI (10  $\mu$ M) (c) Blank in PBS solution upon the green LED irradiation (50  $\text{mW}/\text{cm}^2$ ) for 600s.

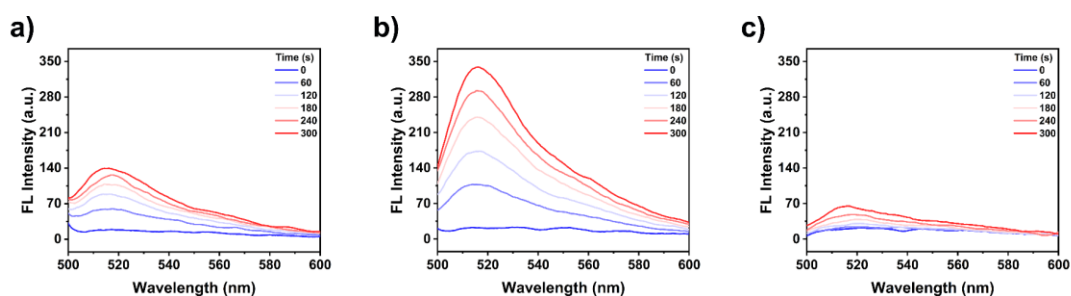


**Figure S14.** The fluorescence spectrum of HPF with (a) FE-VSM (10  $\mu$ M), (b) FE-TMI (10  $\mu$ M) (c) Blank in PBS solution upon the green LED irradiation (50  $\text{mW}/\text{cm}^2$ ) for 300s.



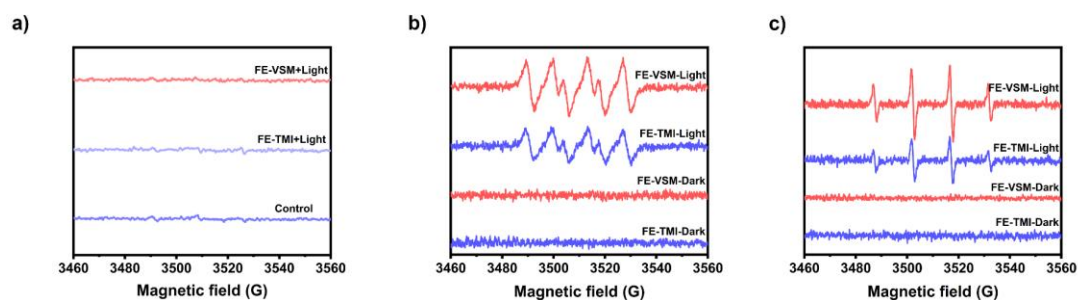


**Figure S15.** (a) EPR spectra for the detection of  $^1\text{O}_2$  using TEMP (water) as a spin trapper. The reaction mixture containing TEMP (100 mM)/FE-TMI (0.5 mg), or TEMP (100 mM)/FE-VSM (0.5 mg) upon green light irradiation for 5 min ( $50\text{mW}/\text{cm}^2$ ). (b) EPR spectra for the detection of  $\bullet\text{OH}$  using DMPO (in 20% acetonitrile–water) as a spin trapper. The reaction mixture containing DMPO (100 mM)/FE-TMI (0.5 mg), or TEMP (100 mM)/FE-VSM (0.5 mg) upon green light irradiation for 5 min ( $50\text{mW}/\text{cm}^2$ ). (c) EPR spectra for the detection of  $\bullet\text{OH}$  using DMPO (in 20% acetonitrile–water) as a spin trapper. The reaction mixture containing TEMP (100 mM)/FE-TMI (0.5 mg), or DMPO (100 mM)/FE-VSM (0.5 mg) upon green light irradiation for 5 min ( $50\text{mW}/\text{cm}^2$ ).

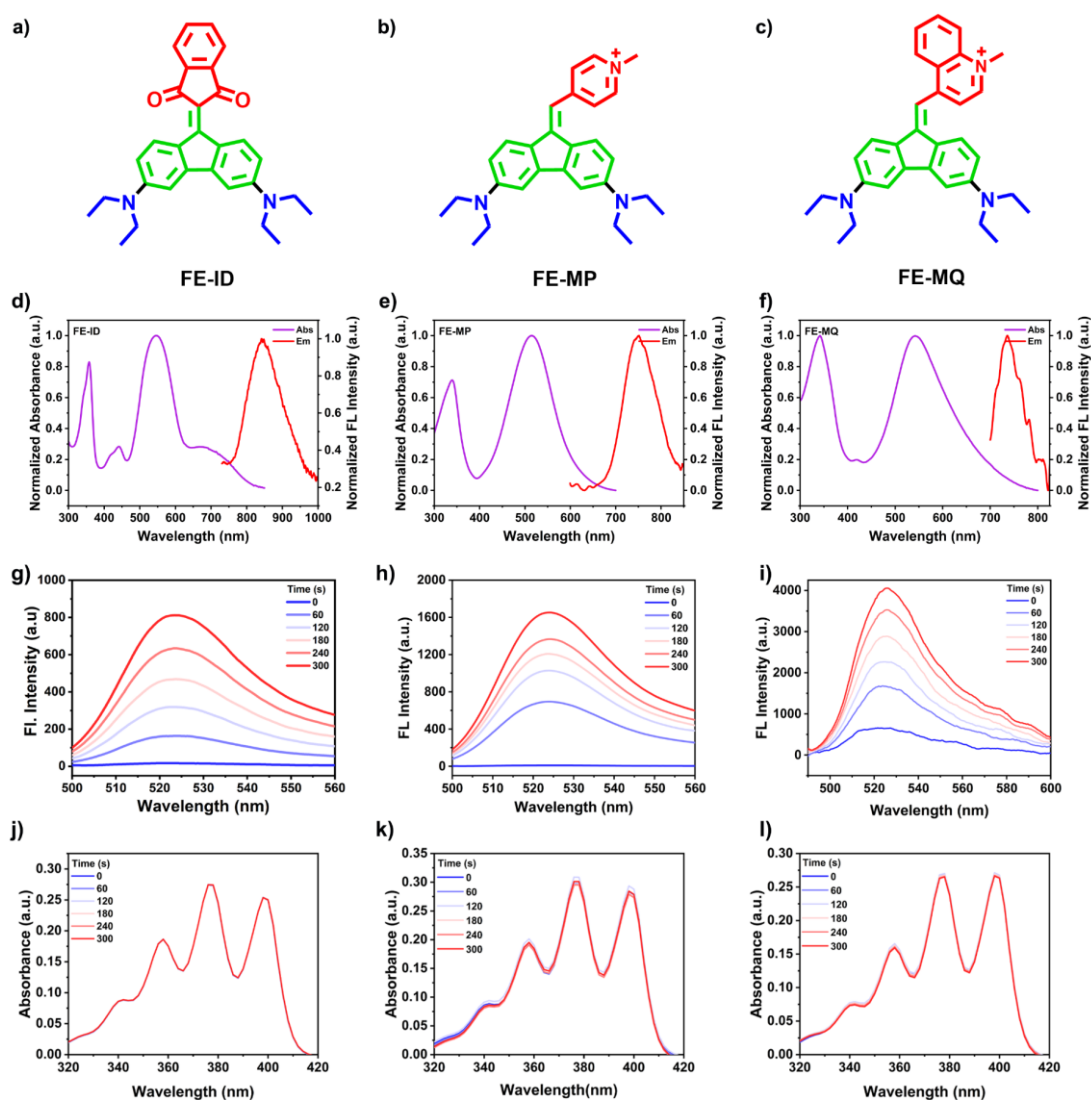


**Figure S16.** The structure of (a) FE-ID, (b) FE-MP and (c) FE-TCF. Normalized absorption and emission spectra of (d) FE-ID, (e) FE-MP and (f) FE-TCF in PBS ( $c = 10 \mu\text{M}$ , Slite = 20 nm). The fluorescence spectrum of DCFH-DA with (g) FE-ID (10  $\mu\text{M}$ ), (h) FE-MP (10  $\mu\text{M}$ ) and (i) FE-MQ (10  $\mu\text{M}$ ) in PBS solution upon the green LED irradiation (50 mW/cm<sup>2</sup>) for 300s. The absorbance spectrum of ABDA with (j) FE-ID (10  $\mu\text{M}$ ), (k) FE-MP (10  $\mu\text{M}$ ) and (l) FE-MQ in PBS solution upon the green LED irradiation (50 mW/cm<sup>2</sup>) for 300s.

**Table S1.** Photophysical properties and photosensitizing properties of FE-VSM, FE-MDN, FE-TCF, and FE-TMI.

Comp.	$\lambda_{\text{abs, PBS}}$ [nm]	$\lambda_{\text{em, PBS}}$ [nm]	HOMO [eV]	LUMO [eV]	$\Delta E_{\text{g}}$ [eV]	$\Delta E_{\text{Sm-Tn}}$ [eV]	QY [%]
FE-VSM	516	873	-6.52	-1.72	4.80	0.13	n.d.
FE-MDN	476	695	-6.48	-1.61	4.87	0.16	6.06
FE-TCF	658	937	-6.42	-1.97	4.45	0.17	n.d.
FE-TMI	558	906	-6.50	-1.79	4.71	0.10	n.d.

**Table S2.** Crystal data and structure refinement for FE-MDN.

CCDC number	2250444
Empirical formula	C <sub>24</sub> H <sub>26</sub> N <sub>4</sub>
Formula weight	370.49
Temperature/K	302.0
Crystal system	monoclinic
Space group	P2 <sub>1</sub> /c
a/Å	10.998(3)
b/Å	11.807(4)
c/Å	16.290(5)
$\alpha$ /°	90
$\beta$ /°	101.724(9)
$\gamma$ /°	90
Volume/Å <sup>3</sup>	2071.2(11)
Z	4
$\rho_{\text{calc}}/\text{g}/\text{cm}^3$	1.188
$\mu/\text{mm}^{-1}$	0.072
F(000)	792.0
Crystal size/mm <sup>3</sup>	0.34 × 0.25 × 0.13
Radiation	MoK $\alpha$ ( $\lambda = 0.71073$ )
2 $\Theta$ range for data collection/°	4.292 to 49.998
Index ranges	-12 ≤ h ≤ 13, -14 ≤ k ≤ 14, -19 ≤ l ≤ 19
Reflections collected	29039
Independent reflections	3633 [ $R_{\text{int}} = 0.0893$ , $R_{\text{sigma}} = 0.0430$ ]
Data/restraints/parameters	3633/0/279
Goodness-of-fit on F <sup>2</sup>	1.022
Final R indexes [ $I \geq 2\sigma(I)$ ]	$R_1 = 0.0476$ , $wR_2 = 0.1068$
Final R indexes [all data]	$R_1 = 0.0856$ , $wR_2 = 0.1319$
Largest diff. peak/hole / e Å <sup>-3</sup>	0.15/-0.19

**Table S3.** Crystal data and structure refinement for FE-TCF.

CCDC number	2250446
Empirical formula	C <sub>33</sub> H <sub>35</sub> Cl <sub>2</sub> N <sub>5</sub> O
Formula weight	588.56
Temperature/K	195.0
Crystal system	monoclinic
Space group	P2 <sub>1</sub> /c
a/Å	14.174(3)
b/Å	11.712(2)
c/Å	19.739(3)
α/°	90
β/°	109.259(6)
γ/°	90
Volume/Å <sup>3</sup>	3093.4(9)
Z	4
ρ <sub>calc</sub> /cm <sup>3</sup>	1.264
μ/mm <sup>-1</sup>	0.244
F(000)	1240.0
Crystal size/mm <sup>3</sup>	0.45 × 0.1 × 0.05
Radiation	MoKα (λ = 0.71073)
2θ range for data collection/°	4.108 to 55.014
Index ranges	-18 ≤ h ≤ 18, -13 ≤ k ≤ 15, -25 ≤ l ≤ 16
Reflections collected	18558
Independent reflections	6919 [R <sub>int</sub> = 0.0720, R <sub>sigma</sub> = 0.0712]
Data/restraints/parameters	6919/12/385
Goodness-of-fit on F <sup>2</sup>	1.024
Final R indexes [I ≥ 2σ (I)]	R <sub>1</sub> = 0.0631, wR <sub>2</sub> = 0.1547
Final R indexes [all data]	R <sub>1</sub> = 0.0971, wR <sub>2</sub> = 0.1800
Largest diff. peak/hole / e Å <sup>-3</sup>	0.53/-0.70

**Table S4.** Crystal data and structure refinement for FE-TMI.

CCDC number	2250445
Empirical formula	C <sub>33</sub> H <sub>40</sub> BrN <sub>3</sub>
Formula weight	558.59
Temperature/K	302.0
Crystal system	triclinic
Space group	P-1
a/Å	10.9276(17)
b/Å	11.2557(14)
c/Å	12.9931(19)
α/°	72.277(5)
β/°	82.974(6)
γ/°	76.606(5)
Volume/Å <sup>3</sup>	1478.6(4)
Z	2
ρ <sub>calc</sub> /cm <sup>3</sup>	1.255
μ/mm <sup>-1</sup>	1.415
F(000)	588.0

Crystal size/mm <sup>3</sup>	0.39 × 0.16 × 0.05
Radiation	MoK $\alpha$ ( $\lambda$ = 0.71073)
2 $\Theta$ range for data collection/ $^{\circ}$	3.882 to 49.998
Index ranges	-12 $\leq$ h $\leq$ 12, -13 $\leq$ k $\leq$ 13, -15 $\leq$ l $\leq$ 15
Reflections collected	17094
Independent reflections	5092 [R <sub>int</sub> = 0.0751, R <sub>sigma</sub> = 0.0584]
Data/restraints/parameters	5092/0/341
Goodness-of-fit on F <sup>2</sup>	1.044
Final R indexes [I $\geq$ 2 $\sigma$ (I)]	R <sub>1</sub> = 0.0824, wR <sub>2</sub> = 0.2334
Final R indexes [all data]	R <sub>1</sub> = 0.1254, wR <sub>2</sub> = 0.2699
Largest diff. peak/hole / e $\text{\AA}^{-3}$	0.81/-0.50

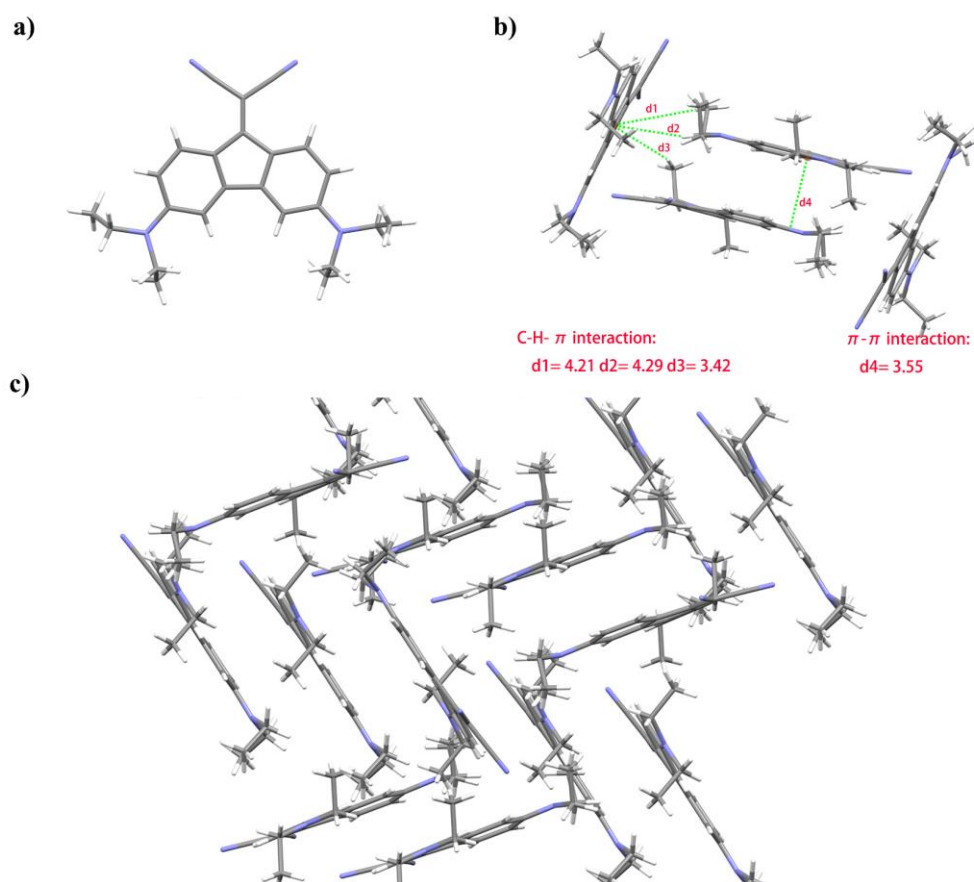


**Figure S17.** Crystal packing of FE-MDN.

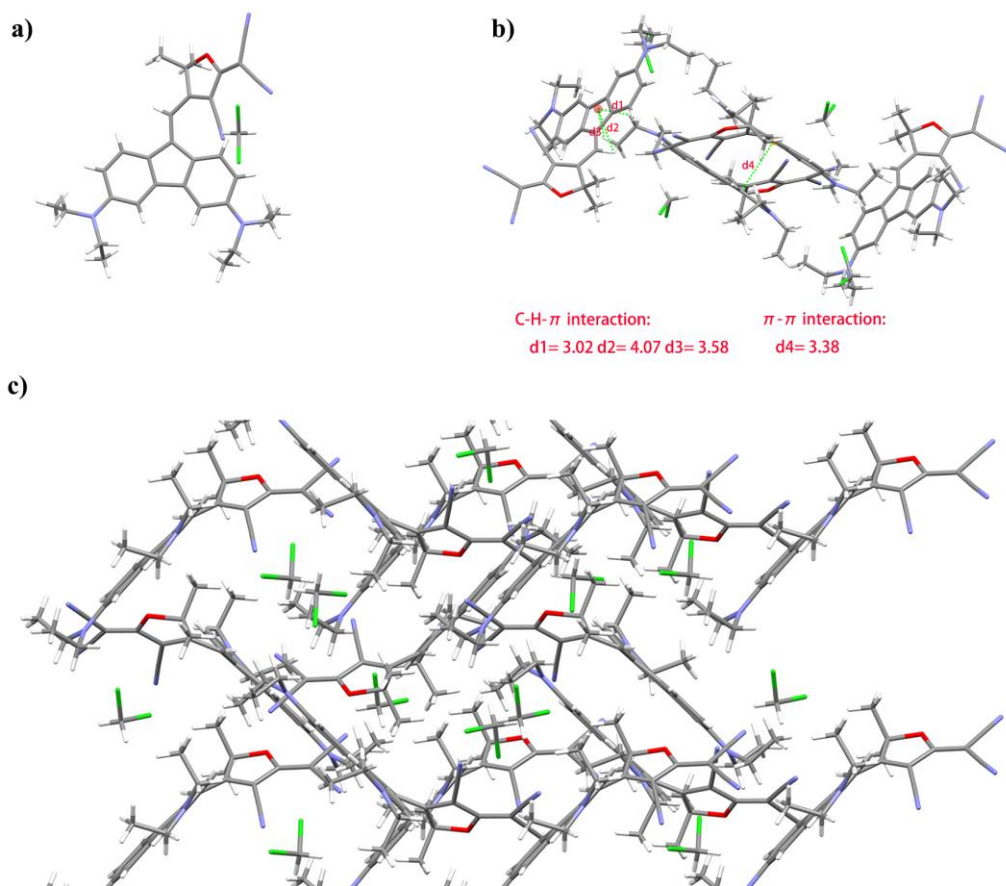


**Figure S18.** Crystal packing of FE-TCF.

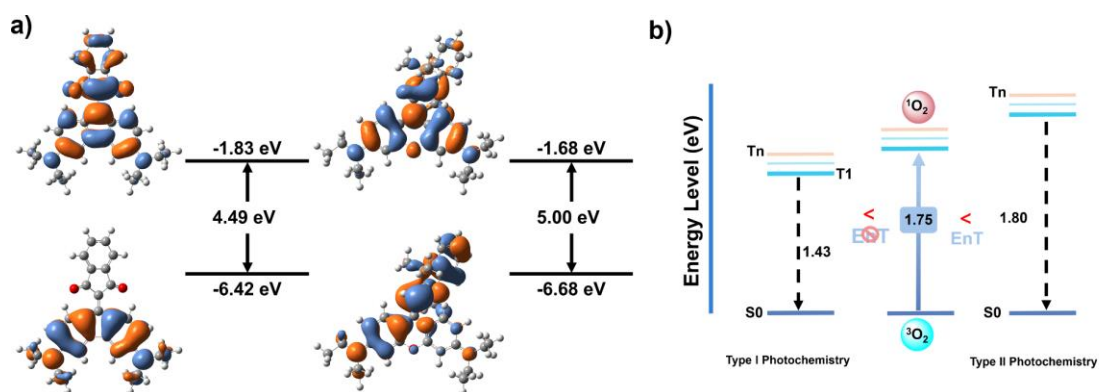
**Table S5.** Time-dependent density functional theory (TD-DFT) calculations of electronic transition energies at the TD-CAM-B3LYP/def2SVP level.

Energy (eV)	FE-VSM	FE-MDN	FE-TCF	FE-TMI	FE-ID	FEO-TMI
S1	1.47	1.76	1.45	2.00	1.94	2.45
S2	2.32	2.72	1.99	2.17	2.52	2.65
S3	2.88	3.09	2.85	2.37	2.92	3.23
S4	3.37	3.73	3.08	2.94	3.06	3.86
S5	3.53	4.02	3.55	3.34	3.07	4.10
T1	0.88	1.21	0.87	1.01	1.43	1.80
T2	1.34	1.59	1.29	1.60	1.67	1.94
T3	2.16	2.42	2.15	2.04	2.60	2.71
T4	2.54	2.91	2.31	2.62	2.63	3.05
T5	2.91	3.12	2.88	2.84	2.78	3.40
$\Delta E_{S1-T1}$	0.59	0.54	0.59	0.99	0.51	0.65
$\Delta E_{S1-T2}$	0.13	0.16	0.18	0.40	0.27	0.50
$\Delta E_{S2-T1}$	1.44	1.51	1.12	1.16	1.09	0.85
$\Delta E_{S2-T2}$	0.98	1.13	0.70	0.57	0.85	0.71
$\Delta E_{S2-T3}$	0.16	0.30	0.16	0.13	0.08	-0.06
$\Delta E_{S3-T1}$	2.00	1.88	1.98	1.36	1.49	1.43
$\Delta E_{S3-T2}$	1.54	1.50	1.56	0.77	1.25	1.29
$\Delta E_{S3-T3}$	0.72	0.67	0.70	0.33	0.32	0.52

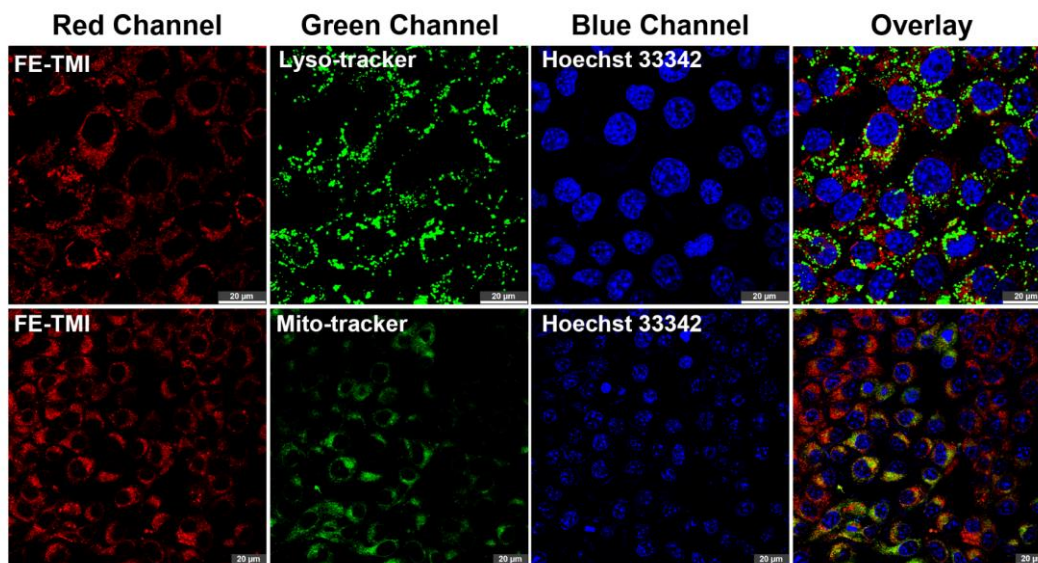
$\Delta E_{S3-T4}$	0.33	0.18	0.54	-0.25	0.29	0.18
$\Delta E_{S4-T1}$	2.49	2.52	2.19	1.93	1.63	2.06
$\Delta E_{S4-T2}$	2.03	2.14	1.79	1.34	1.59	1.92
$\Delta E_{S4-T3}$	1.21	1.31	0.93	0.90	1.40	1.15
$\Delta E_{S4-T4}$	0.83	0.82	0.77	0.32	0.43	0.81
$\Delta E_{S4-T5}$	0.46	0.61	0.20	0.10	0.28	0.46

**Table S6.** Calculated spin-orbit coupling (SOC) constants between singlet and triplet states of FE-VSM, FE-MDN, FE-TCF and FE-TMI.

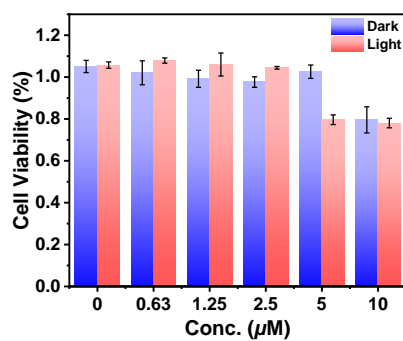
$\langle S_n   H_{SO}   T_m \rangle$	FE-VSM	FE-MDN	FE-TCF	FE-TMI
S1-T1	0.02	0.01	0.06	283.35
S1-T2	0.78	0.18	0.52	369.89
S2-T1	1.21	0.05	0.57	407.13
S2-T2	0.89	0.03	0.11	178.19
S2-T3	0.06	0.18	0.18	33.39
S3-T1	0.08	0.33	0.13	76.73
S3-T2	0.02	0.14	0.23	75.26
S3-T3	0.10	0.12	0.11	6.52
S3-T4	0.33	0.01	0.09	90.20
S4-T1	0.35	0.22	0.06	629.64
S4-T2	1.31	0.05	0.32	613.01
S4-T3	0.27	0.02	0.09	18.09
S4-T4	0.03	0.13	0.26	229.00
S4-T5	0.16	0.04	0.01	238.84



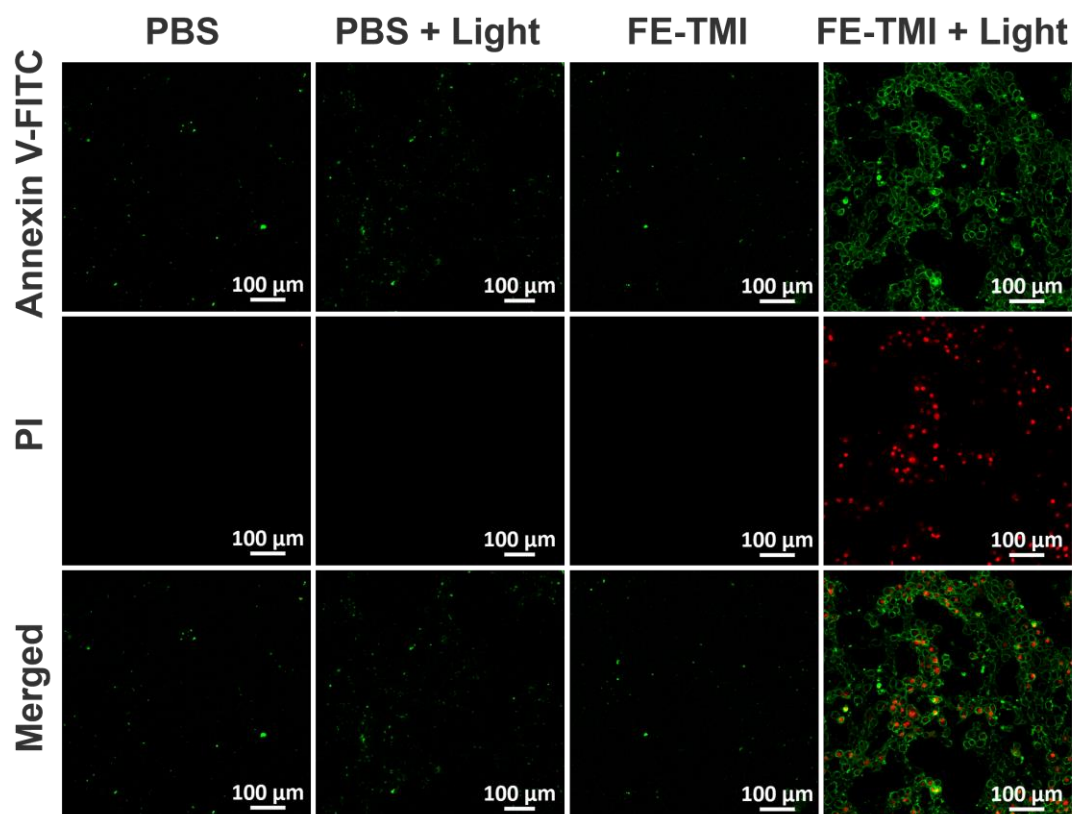
**Figure S19.** (a) HOMO-LUMO distribution of FE-ID, O-FE in their ground state (S0). (b) Energy profile for a putative Type-II energy transfer from the T1 levels of FE-ID, O-FE to <sup>3</sup>O<sub>2</sub>.



**Figure S20.** Confocal fluorescence images of 4T-1 cells co-stained with 5  $\mu\text{M}$  FE-TMI, 0.5  $\mu\text{M}$  Hoechst 33342, and 1  $\mu\text{M}$  Lyso-tracker Green, and 1  $\mu\text{M}$  Mito-tracker Green (red channel:  $\lambda_{\text{ex}}$  = 560 nm and  $\lambda_{\text{em}}$  = 700–850 nm; green channel:  $\lambda_{\text{ex}}$  = 488 nm and  $\lambda_{\text{em}}$  = 500–520 nm; blue channel:  $\lambda_{\text{ex}}$  = 405 nm and  $\lambda_{\text{em}}$  = 460–490 nm).



**Figure S21.** Cell viability of 4T-1 cells in the presence of light irradiation or dark conditions.

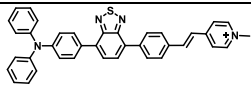
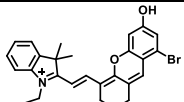
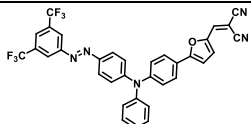
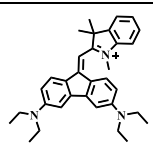


**Figure S22.** Cell apoptosis of 4T-1 cells in the presence of light irradiation under normoxia conditions.

**Table S5.** Recently published Type-I photosensitizers of organic small-molecules and their IC<sub>50</sub>.

Entry	Structure	IC <sub>50</sub>	Illumination condition	Ref.
1		10.3 $\mu\text{M}$ (1% O <sub>2</sub> ) MCF-7 Cells	White-light 20 mW/cm <sup>2</sup> 10 min	<i>Nat. Commun.</i> <b>2022</b> , 13, 2225
2		188.4 $\mu\text{M}$ (21 % O <sub>2</sub> ) 212.7 $\mu\text{M}$ (1 % O <sub>2</sub> ) MCF-7 Cells	White light 25 mW/cm <sup>2</sup> 30 min	<i>ACS Nano</i> <b>2023</b> , 17, 9110-9125
3		0.0675 $\mu\text{M}$ (2% O <sub>2</sub> ) MCF-7 Cells	660 nm 20 mW/cm <sup>2</sup> 5 min	<i>J. Am. Chem. Soc.</i> <b>2020</b> , 142, 5380–5388
4		0.39 $\mu\text{M}$ (21% O <sub>2</sub> ) 0.56 $\mu\text{M}$ (2% O <sub>2</sub> ) HepG2 Cells	730 nm 50 mW/cm <sup>2</sup> 10 min	<i>Angew. Chem.</i> <i>Int. Ed.</i> <b>2021</b> , 60, 19912–19920



5		n.d. 4T-1 Cells	White light 100 mW/cm <sup>2</sup>	<i>Aggregate</i> <b>2024</b> , e612
6		2.9 μM (21 % O <sub>2</sub> ) 2.6 μM (2 % O <sub>2</sub> ) 4T-1 Cells	660 nm 50 mW/cm <sup>2</sup> 10 min	<i>Adv. Mater.</i> <b>2024</b> , 36, 2305243
7		3.217 μM (< 0.5% O <sub>2</sub> ) MCF-7 Cells	White light 40 mW/cm <sup>2</sup> 30 min	<i>Angew. Chem. Int. Ed.</i> <b>2023</b> , 62, e202307288
8		<b>0.052 μM (21% O<sub>2</sub>)</b> <b>0.11 μM (&lt;1% O<sub>2</sub>)</b> 4T-1 Cells	<b>Green light</b> <b>50 mW/cm<sup>2</sup></b> <b>5 min</b>	<b>This Work</b>

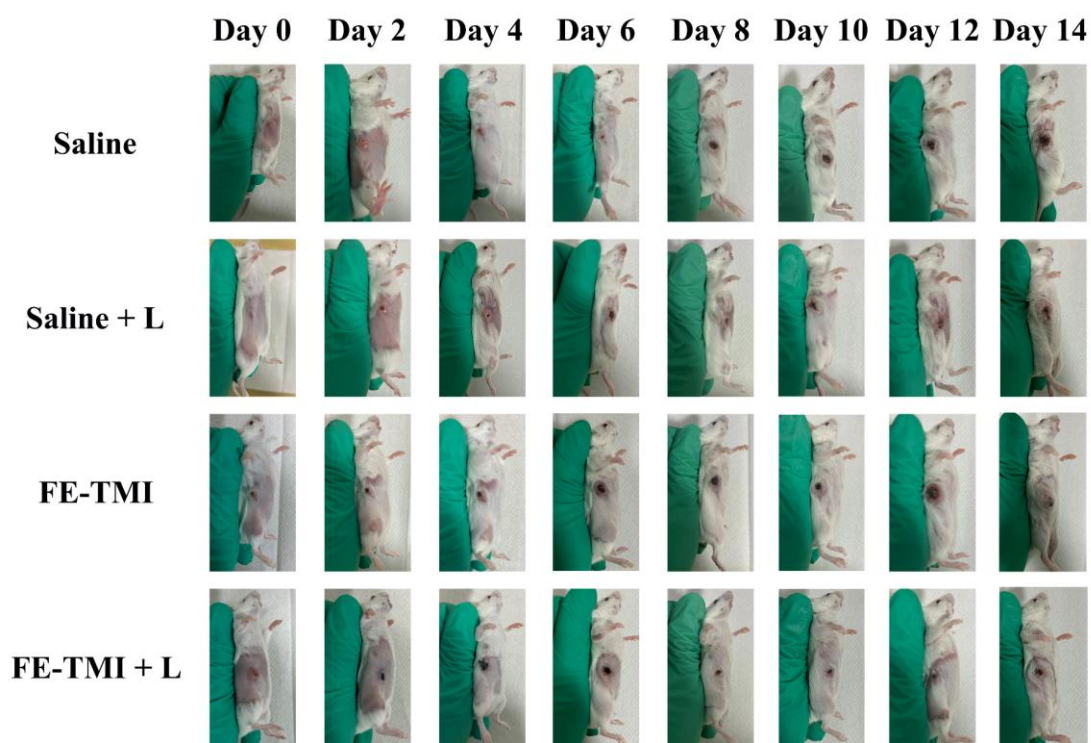


**Figure S23.** The picture of mice at different times after treatment.

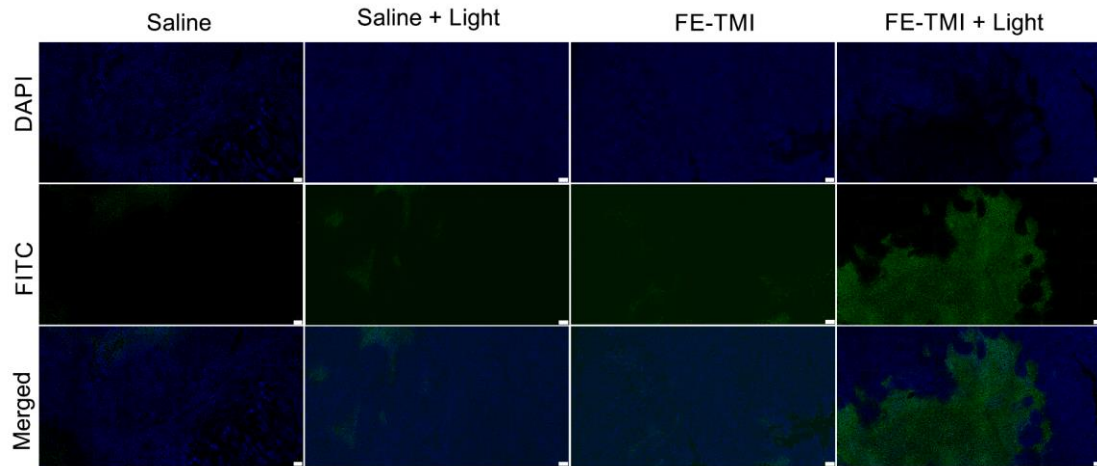


**Figure S24.** The TUNEL staining with tumor under the different treatment, scale bar = 100  $\mu$ m.

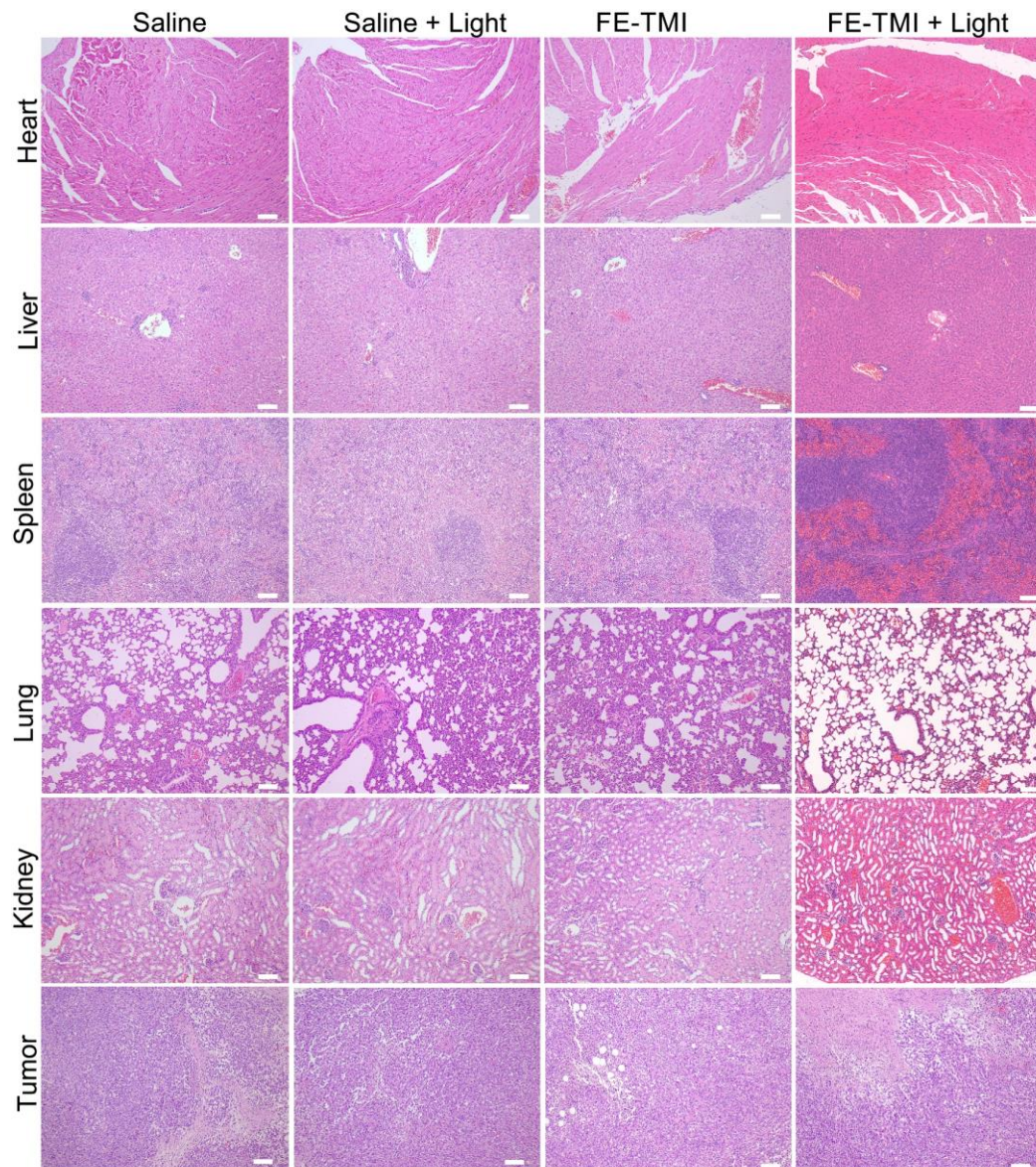


**Figure S25.** The H&E staining with heart, liver, spleen, lung, kidney, and tumor under the different treatment, scale bar = 100  $\mu$ m.

## Theoretical calculation data

FE-VSM Geometry and Frequency Data Total Energy of FE-VSM: -2214.60627642 Hartrees

Zero imaginary frequencies were found from the optimized geometry of FE-VSM.

XYZ Coordinates of FE-VSM

```
0 1
C      -3.45016933  0.32183457  0.36011335
C      -3.07907152  1.69690844  0.26009508
C      -1.68259157  1.96672250  0.15015397
C      -0.78358821  0.93422749  0.03643454
C      -1.17616602 -0.42197958  0.03741276
C      -2.52457137 -0.70590829  0.25168817
C      0.69115374  0.97811951 -0.02965183
C      1.16375002 -0.35239676 -0.03210448
C      0.01938109 -1.27245437  0.00216650
C      1.52809516  2.06352808 -0.14255689
C      2.94378430  1.87195617 -0.25287410
C      3.38957376  0.52682671 -0.35359002
C      2.52804141 -0.55383042 -0.24691721
N      -3.98295228  2.73347195  0.30573539
N      3.83748631  2.91662351 -0.30279908
C      -3.37877010  4.06557383  0.45709944
C      -5.38018155  2.39513838  0.62585759
C      3.27623232  4.27082843 -0.45872974
C      5.21724627  2.53169862 -0.62865518
C      0.05526029 -2.65081860  0.00109013
C      -6.48014965  3.42166955  0.42048425
C      -4.23387827  5.31248708  0.33010648
C      4.17441310  5.48801364 -0.34037036
C      6.35328506  3.51977605 -0.43033611
S      1.34063412 -3.63144696  0.74439823
S      -1.18266060 -3.68642901 -0.74649321
C      1.85660406 -2.70114177  2.16022353
C      -1.74097616 -2.77232771 -2.15658924
C      -3.03580162 -2.67169387 -2.41767216
C      3.14536805 -2.54224421  2.42214485
O      0.65843359 -4.81763826  1.28657117
O      2.49457394 -3.85815497 -0.13956355
O      -0.44656193 -4.83705749 -1.29502317
O      -2.32427532 -3.97071294  0.13627855
H      -4.47811965  0.03473238  0.54288452
H      -1.29783640  2.98379413  0.17533810
```

H	-2.87406901	-1.73100984	0.36786044
H	1.08212847	3.05073351	-0.16694897
H	4.43794652	0.30435342	-0.53685027
H	2.93917392	-1.55508471	-0.36453895
H	-2.83608757	4.10946595	1.41904263
H	-2.61299007	4.14912596	-0.32568773
H	-5.64466058	1.55165630	-0.01998241
H	-5.43995418	2.01449318	1.66236514
H	2.73301175	4.33061816	-1.41941143
H	2.51863013	4.38574819	0.32430086
H	5.45451196	1.67811592	0.01951768
H	5.25720165	2.14620696	-1.66432154
H	-7.43516223	2.88507802	0.52298227
H	-6.48108365	4.22392193	1.16569529
H	-6.45802464	3.86629358	-0.58306926
H	-3.54173284	6.16765614	0.32515715
H	-4.79971664	5.34108308	-0.61032897
H	-4.92463544	5.46257085	1.16639629
H	3.51251160	6.36685608	-0.33736573
H	4.74446140	5.50201292	0.59737254
H	4.86674099	5.60939711	-1.18061719
H	7.28839011	2.94947723	-0.53398368
H	6.38082377	4.31951836	-1.17708040
H	6.34949901	3.96753923	0.57256136
H	1.03228365	-2.40248593	2.81250564
H	-0.93140438	-2.43188548	-2.80676747
H	-3.37603151	-2.20270688	-3.34460914
H	-3.79076359	-3.05094524	-1.72433957
H	3.46362489	-2.06366650	3.35195717
H	3.91701637	-2.88188801	1.72668724

FE-MDN Geometry and Frequency Data Total Energy of FE-MDN: -1147.73104572 Hartrees

Zero imaginary frequencies were found from the optimized geometry of FE-MDN.

XYZ Coordinates of FE-MDN

0 1			
N	10.31279237	-7.19747846	-2.78481953
N	2.15836066	-7.23922274	-6.66026004
N	3.66217680	-9.02712667	-2.91623759
N	7.41826256	-4.28152129	-9.38861016
C	11.02143132	-9.45188816	-2.04648490
H	10.22733565	-9.90424736	-2.60537112
H	11.23997220	-10.06267883	-1.19159508

H	11.89495779	-9.38797912	-2.66314540
C	10.59870365	-8.02849077	-1.59606740
H	9.72243990	-8.08870825	-0.98068782
H	11.39539290	-7.57351026	-1.03001699
C	9.07650679	-7.16553642	-3.32748618
C	8.79682082	-6.35102821	-4.47392147
H	9.55024390	-5.72051014	-4.92671552
C	7.53477860	-6.42284933	-4.98761659
C	6.91830250	-5.75730485	-6.25766644
C	7.51441876	-5.04296060	-7.21215435
H	8.55802420	-4.77321591	-7.13491669
C	6.72585052	-4.66138709	-8.33075199
C	6.96845039	-3.30829846	-10.43857340
H	6.40519893	-3.81994390	-11.18056764
H	7.84552026	-2.87708459	-10.89064557
C	6.08476093	-2.17755580	-9.84649858
H	5.20606298	-2.58063012	-9.38146558
H	5.78191175	-1.50716469	-10.62334147
H	6.65122573	-1.65190398	-9.12417435
C	11.47281119	-5.02508177	-2.67749225
H	10.54825416	-4.50989007	-2.82753112
H	12.27255001	-4.44607299	-3.09420225
H	11.64255905	-5.16008674	-1.63002926
C	11.40918061	-6.41758472	-3.37033693
H	11.23928578	-6.29220341	-4.41910339
H	12.33561269	-6.93770323	-3.21557429
C	8.04159850	-7.94663836	-2.72179079
H	8.26177886	-8.54001914	-1.85480090
C	6.77564356	-7.95303442	-3.24544961
H	5.98111189	-8.53626560	-2.80376211
C	6.54528596	-7.18268087	-4.38616450
C	5.57110870	-6.04928074	-6.34046449
C	5.23695669	-7.00705917	-5.19383088
C	4.02496618	-7.59867237	-4.97117803
C	2.99517947	-7.41023565	-5.88721000
C	3.82605484	-8.38087880	-3.84606394
C	4.72972753	-5.49906009	-7.32606069
H	3.66795725	-5.67841379	-7.31399453
C	5.31333850	-4.76593359	-8.32425068
H	4.71763254	-4.29577400	-9.08730080
C	8.67025909	-5.07841793	-9.45863462
C	9.96461102	-4.27569658	-9.40664312
H	8.65735557	-5.63307430	-10.37106698
H	8.67135452	-5.73819928	-8.61676704

H	10.77755180	-4.97254251	-9.42148043
H	10.03014386	-3.62654006	-10.24624627
H	9.99830972	-3.70618064	-8.50287341

FE-TCF Geometry and Frequency Data Total Energy of FE-TCF: -1586.20094978 Hartrees

Zero imaginary frequencies were found from the optimized geometry of FE-TCF.

XYZ Coordinates of FE-TCF

0 1

O	4.82503417	-1.85095343	0.80768216
N	5.86316660	1.58114998	-2.32059697
N	8.13626007	-1.08998046	0.25427929
N	2.46433138	0.65512577	-2.41561666
N	-1.31362542	4.45099684	-0.08328936
C	-3.98032168	-1.99144877	-0.50146646
C	-3.06832532	-3.04648445	-0.26335212
H	-3.41427834	-4.06727270	-0.25430108
C	-1.72753438	-2.81169666	-0.03729632
H	-1.07014790	-3.65615969	0.12811722
C	-1.24428598	-1.51318705	-0.01681913
C	0.10644905	-0.98424932	0.14912581
C	1.18058740	-1.80189262	0.39949622
H	0.92849628	-2.81185392	0.70300856
C	2.56232070	-1.55711890	0.34784967
C	3.32358770	-0.71356159	-0.43381877
C	4.70304378	-0.91639215	-0.11512575
C	5.84655700	-0.32102544	-0.60586702
C	5.83092626	0.72294832	-1.55465145
C	7.10715341	-0.74696756	-0.13002106
C	3.51484419	-2.38441755	1.17918216
C	3.51218490	-3.85613831	0.81532543
H	3.66440120	-3.99128020	-0.25473563
H	2.56469855	-4.30936288	1.10037009
H	4.31202395	-4.35848887	1.35786497
C	3.33350915	-2.14788204	2.66488926
H	4.11035488	-2.67625858	3.21598689
H	2.36191568	-2.52857224	2.97611444
H	3.38689906	-1.08502197	2.89747896
C	2.85805876	0.06175042	-1.51366786
C	-0.02463123	0.46612745	0.08910680
C	-1.37570607	0.79674450	-0.14121772
C	-2.14214894	-0.45883210	-0.23264681
C	-3.47420334	-0.66695915	-0.46727125
H	-4.12412964	0.17914739	-0.62680621

C	-5.82847226	-3.59020612	-0.76536422
H	-5.13007676	-4.25413640	-1.27433601
H	-6.73173692	-3.57915067	-1.37325377
C	-6.15533922	-4.13849798	0.61510455
H	-5.27905221	-4.14009340	1.26372729
H	-6.51124236	-5.16632126	0.52626669
H	-6.93619471	-3.55101149	1.09733097
C	-1.82335533	2.08725340	-0.18400266
H	-2.87258823	2.27789719	-0.34687901
C	-0.91135353	3.15586726	0.01471358
C	-0.39447324	5.54982075	0.18913265
H	-0.79466753	6.42891783	-0.31329103
H	0.56264764	5.33784742	-0.28697376
C	-0.18555564	5.86039794	1.66326683
H	-1.11402511	6.18276944	2.13364411
H	0.54417321	6.66503270	1.76776310
H	0.18942807	4.99274955	2.20649878
C	-2.71551286	4.79345426	-0.29582097
H	-3.12716025	4.14784807	-1.07147947
H	-2.73573489	5.80385557	-0.70037342
C	-3.58632781	4.73044981	0.94948830
H	-3.57510744	3.73681300	1.39794105
H	-4.61803845	4.96984898	0.68660137
H	-3.25321721	5.44699626	1.69967801
C	0.42793923	2.81688581	0.31537319
H	1.14557911	3.59090262	0.53328472
C	0.85816424	1.50767868	0.34674805
H	1.89109022	1.31959842	0.60156626
N	-5.29245592	-2.23468531	-0.77844608
C	-6.25158958	-1.14338615	-0.90546821
C	-6.70238139	-0.52897612	0.41084005
H	-7.11610698	-1.54385611	-1.43189889
H	-5.83488970	-0.37140821	-1.55305712
H	-7.39296098	0.29268480	0.21360897
H	-7.21650688	-1.26204480	1.03181575
H	-5.86070307	-0.13158743	0.97835952

FE-TMI Geometry and Frequency Data Total Energy of FE-TMI: -1561.62701618 Hartrees

Zero imaginary frequencies were found from the optimized geometry of FE-TMI.

XYZ Coordinates of FE-TMI

1	1		
C	0	2.969321	1.044639 -1.304911
C	0	2.789287	2.267104 -0.763922

C 0	1.526971	2.443186	-0.313143
C 0	0.528889	1.535409	-0.351682
C 0	0.781420	0.301347	-0.820645
C 0	2.008734	0.109746	-1.339959
C 0	-1.860094	0.779917	-0.092403
C 0	-1.458836	-0.413535	-0.567261
C 0	-0.162815	-0.663839	-0.862184
C 0	-3.159488	0.961224	0.225211
C 0	-4.151932	0.051264	0.106562
C 0	-3.698852	-1.132256	-0.355701
C 0	-2.414044	-1.357437	-0.667828
N 0	3.714933	3.163764	-0.707106
N 0	-5.384874	0.274901	0.414496
C 0	3.331193	4.519422	-0.195042
C 0	5.087946	2.765552	-1.159667
C 0	-6.334115	-0.882851	0.336455
C 0	-5.753053	1.673120	0.812478
C 0	0.191717	-1.893720	-1.284960
C 0	6.325033	3.602266	-0.807173
C 0	4.247544	5.737078	-0.373501
C 0	-7.730620	-0.823374	0.969431
C 0	-7.214355	2.140018	0.849887
C 0	1.034643	-2.756800	-0.678222
C 0	1.615003	-2.623838	0.735262
C 0	2.212795	-4.003432	0.794109
C 0	2.004348	-4.665498	-0.349153
N 0	1.319766	-3.934595	-1.189708
C 0	2.877758	-4.562224	1.815851
C 0	3.347139	-5.812018	1.678339
C 0	3.143596	-6.484512	0.533948
C 0	2.469503	-5.918097	-0.480924
C 0	2.729092	-1.598248	0.982611
C 0	0.496974	-2.481615	1.782054
C 0	0.907043	-4.395084	-2.578314
C 0	-0.860765	1.909216	0.155057
C 0	-1.339932	3.170922	-0.606816
C 0	-0.773860	2.166237	1.676005
H 0	3.913784	0.728102	-1.774278
H 0	1.244557	3.394005	0.152953
H 0	2.283210	-0.837049	-1.835889
H 0	-3.380833	1.947623	0.648201
H 0	-4.354417	-2.001807	-0.519362
H 0	-2.189009	-2.380952	-1.011399
H 0	2.409378	4.853661	-0.735715



H 0	3.117512	4.440331	0.899617
H 0	5.345922	1.782820	-0.689435
H 0	5.078854	2.657158	-2.272275
H 0	-6.482361	-1.150756	-0.738820
H 0	-5.879562	-1.749579	0.880055
H 0	-5.325053	1.880355	1.824349
H 0	-5.314846	2.382991	0.065614
H 0	-0.369138	-2.275011	-2.154970
H 0	7.259580	3.063654	-1.091378
H 0	6.368367	4.560428	-1.368125
H 0	6.390180	3.792500	0.288333
H 0	3.724905	6.672435	-0.063323
H 0	5.152160	5.689319	0.270146
H 0	4.537961	5.876583	-1.439645
H 0	-8.220862	-1.824796	0.937395
H 0	-7.680255	-0.530719	2.042876
H 0	-8.421861	-0.150410	0.417959
H 0	-7.272283	3.241812	1.014150
H 0	-7.732522	1.936693	-0.114835
H 0	-7.784119	1.696690	1.694583
H 0	3.038423	-4.010408	2.755022
H 0	3.896641	-6.287954	2.507731
H 0	3.526734	-7.513923	0.430799
H 0	2.309021	-6.505454	-1.397470
H 0	3.223663	-1.763464	1.965576
H 0	3.524332	-1.655815	0.205667
H 0	2.336006	-0.562265	1.045064
H 0	0.004272	-1.486039	1.719489
H 0	-0.290158	-3.258390	1.648271
H 0	0.894298	-2.578845	2.817434
H 0	-0.159358	-4.716395	-2.574221
H 0	1.053546	-3.584363	-3.327057
H 0	1.523281	-5.241210	-2.948690
H 0	-1.396331	2.968408	-1.701142
H 0	-2.339267	3.533436	-0.284986
H 0	-0.679059	4.052653	-0.466626
H 0	-0.071307	2.989119	1.932463
H 0	-1.750932	2.459568	2.118465
H 0	-0.426062	1.251904	2.209898

FE-ID Geometry and Frequency Data Total Energy of FE-ID: -1419.44536857 Hartrees

Zero imaginary frequencies were found from the optimized geometry of FE-ID.

XYZ Coordinates of FE-ID

0 1

N	-1.49673173	4.56803622	0.04770498
C	-4.06758170	-1.85586509	-0.64737678
C	-3.12134458	-2.90949442	-0.75523479
H	-3.45929861	-3.92031331	-0.85146176
C	-1.78180394	-2.64026596	-0.73653536
H	-1.06087852	-3.42575741	-0.82175330
C	-1.39612700	-1.35638449	-0.60652470
C	0.02134355	-0.76749982	-0.54608596
C	-0.17200562	0.74757494	-0.38165733
C	-1.52850700	1.01213857	-0.35739175
C	-2.30234266	-0.31502435	-0.49978475
C	-3.62838764	-0.52446571	-0.52364780
H	-4.32226213	0.28675845	-0.44946006
C	-5.83253793	-3.52297349	-0.74295048
H	-5.11714050	-4.10273315	-1.28688392
H	-6.77685791	-3.56051076	-1.24460555
C	-5.98197524	-4.09431424	0.67920854
H	-5.03654218	-4.05812233	1.17875720
H	-6.31735725	-5.10886111	0.62326053
H	-6.69577276	-3.51230622	1.22395508
C	-2.00428449	2.26196146	-0.22357557
H	-3.05668498	2.45544324	-0.21085614
C	-1.06752675	3.30988976	-0.09788194
C	-0.52804900	5.65792672	0.22546342
H	-0.93079823	6.56250005	-0.17875193
H	0.38182781	5.41506932	-0.28258616
C	-0.24369136	5.84610632	1.72674448
H	-1.15465894	6.08464651	2.23460310
H	0.45847301	6.64208426	1.86033866
H	0.16218755	4.94116831	2.12866277
C	-2.93713950	4.86102012	0.03095774
H	-3.43661029	4.15434539	-0.59732187
H	-3.09428808	5.84936974	-0.34754322
C	-3.50196044	4.76298371	1.46038803
H	-3.34555234	3.77436307	1.83829095
H	-4.55041224	4.97722422	1.44473946
H	-3.00318745	5.46888253	2.09094306
C	0.32797362	3.03659645	-0.12337341
H	1.02919715	3.83972591	-0.02953960
C	0.77827795	1.75592503	-0.26749449
H	1.82531396	1.53622778	-0.29127814
N	-5.37566507	-2.12900407	-0.66137437
C	-6.35700940	-1.03627229	-0.59410064

C	-6.68794622	-0.72829853	0.87814103
H	-7.24960357	-1.32772628	-1.10683645
H	-5.94877741	-0.16255306	-1.05634113
H	-7.40308802	0.06671068	0.92382094
H	-7.09514679	-1.60147824	1.34291907
H	-5.79546701	-0.43477098	1.39017214
C	1.19281593	-1.44339946	-0.62138155
C	3.61711267	-1.97697728	-0.67889245
C	2.85454939	-3.27730431	-0.82608389
C	3.47945346	-4.46132591	-0.95877549
H	2.92585210	-5.37176234	-1.06271500
C	5.72136938	-3.27817889	-0.82486652
H	6.79139672	-3.28624000	-0.82717879
C	4.96138222	-1.93559796	-0.67254225
H	5.48687609	-1.00906513	-0.56688385
C	5.02970580	-4.45765480	-0.95667933
H	5.56446129	-5.37912606	-1.05905720
C	1.34872353	-2.97062581	-0.79460280
C	2.60690501	-0.82471714	-0.55065725
O	0.41538003	-3.80827891	-0.89263605
O	2.88100731	0.39611667	-0.41335054

FEO-TMI Geometry and Frequency Data Total Energy of FEO-TMI: -1519.01105768 Hartrees

Zero imaginary frequencies were found from the optimized geometry of FEO-TMI.

XYZ Coordinates of FEO-TMI

1 1			
N	6.01233124	-0.54136675	0.20104475
N	-2.20593013	-1.84354803	-0.84941097
N	-2.76275936	4.31307156	-0.17764749
C	6.86415828	0.53738660	-1.88648970
H	7.36128295	-0.38170088	-2.23205132
H	7.44966497	1.39652754	-2.24702823
H	5.86931739	0.58376117	-2.35435946
C	6.76925204	0.57026581	-0.36781829
H	7.77358029	0.55796090	0.06854018
H	6.32220744	1.51352635	-0.03025632
C	4.65191688	-0.50624359	0.21370025
C	3.87884554	-1.65892869	0.55083074
H	4.36329324	-2.60964242	0.75633232
C	2.51231545	-1.60483968	0.61097271
H	1.98463152	-2.52479027	0.85644695
C	1.76456132	-0.42319560	0.36220968
C	0.32508218	-0.40954813	0.45095273

C	-0.35175052	-1.63496277	0.76494364
H	0.14956702	-2.28309556	1.48440074
C	-1.52563641	-2.16735585	0.28203321
C	-2.22656134	-3.34787224	0.96738147
C	-3.43168267	-3.54189484	0.07449750
C	-4.48565344	-4.43610979	0.15381644
H	-4.54130319	-5.16171844	0.96862930
C	-5.48330375	-4.39352444	-0.82746278
H	-6.32426631	-5.08791099	-0.77654396
C	-5.41130643	-3.46759730	-1.86687778
H	-6.19818512	-3.44141420	-2.62382285
C	-4.34915895	-2.56316584	-1.95846200
H	-4.30307513	-1.83583486	-2.76960630
C	-3.37016621	-2.62596502	-0.97556332
C	-2.63323156	-2.97472812	2.39797751
H	-1.74394671	-2.77906726	3.01459291
H	-3.19346397	-3.80344102	2.85554082
H	-3.27072509	-2.07863173	2.41150286
C	-1.33459137	-4.59775091	0.97134020
H	-1.00883460	-4.85885142	-0.04588475
H	-1.89520845	-5.44916235	1.38416198
H	-0.44308064	-4.44222930	1.59626200
C	-1.75149309	-0.96168052	-1.90094449
H	-0.65495999	-0.93524855	-1.90932716
H	-2.12850081	0.06436199	-1.78097110
H	-2.09391732	-1.35309650	-2.86734826
C	6.68798253	-1.83114052	0.39860047
H	6.27704301	-2.29435702	1.30587308
H	6.44344374	-2.51144853	-0.43655191
C	8.19403130	-1.75483840	0.55914502
H	8.70412917	-1.40098480	-0.34755037
H	8.56530190	-2.76764987	0.77232425
H	8.48477954	-1.10896101	1.40070906
C	3.92330816	0.65915376	-0.10867031
H	4.44280415	1.55925033	-0.43094668
C	2.53647088	0.70068438	-0.02945767
C	0.13848293	2.03291035	-0.14814461
C	-0.62504517	3.18176978	-0.30760895
H	-0.12953492	4.07778356	-0.67581992
C	-1.99738635	3.21375319	0.02864492
C	-2.53296892	2.02666971	0.61934824
H	-3.55176762	2.00998007	0.99832970
C	-1.77251350	0.89863814	0.74902895
H	-2.22046429	0.03384766	1.23576431

C	-0.41663293	0.81342413	0.32447924
C	-2.18492363	5.54984356	-0.69987672
H	-3.00799182	6.12112934	-1.14908174
H	-1.50236175	5.30395748	-1.52594393
C	-1.47054688	6.41114292	0.33324537
H	-2.16101232	6.74883135	1.11901882
H	-1.05002697	7.30254824	-0.15613963
H	-0.64340272	5.86868375	0.81450880
C	-4.16376388	4.35447111	0.23992014
H	-4.64066093	3.39671072	-0.01011988
H	-4.65821891	5.10977276	-0.38523204
C	-4.38599037	4.68298886	1.70977257
H	-3.89922271	3.94807880	2.36794405
H	-5.46381447	4.67417660	1.93166838
H	-3.99558926	5.67925851	1.96159205
O	1.82339981	2.20446450	-0.55501543

# NMR SPECTRA

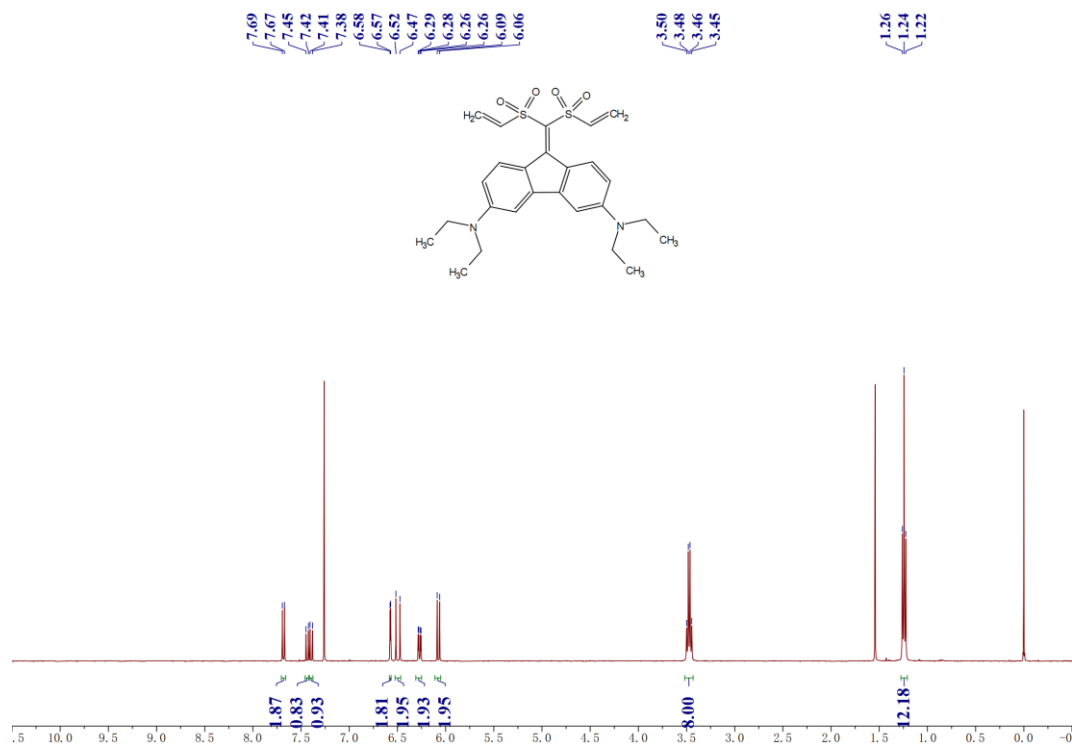


Figure S26. The <sup>1</sup>H NMR spectra of FE-VSM.

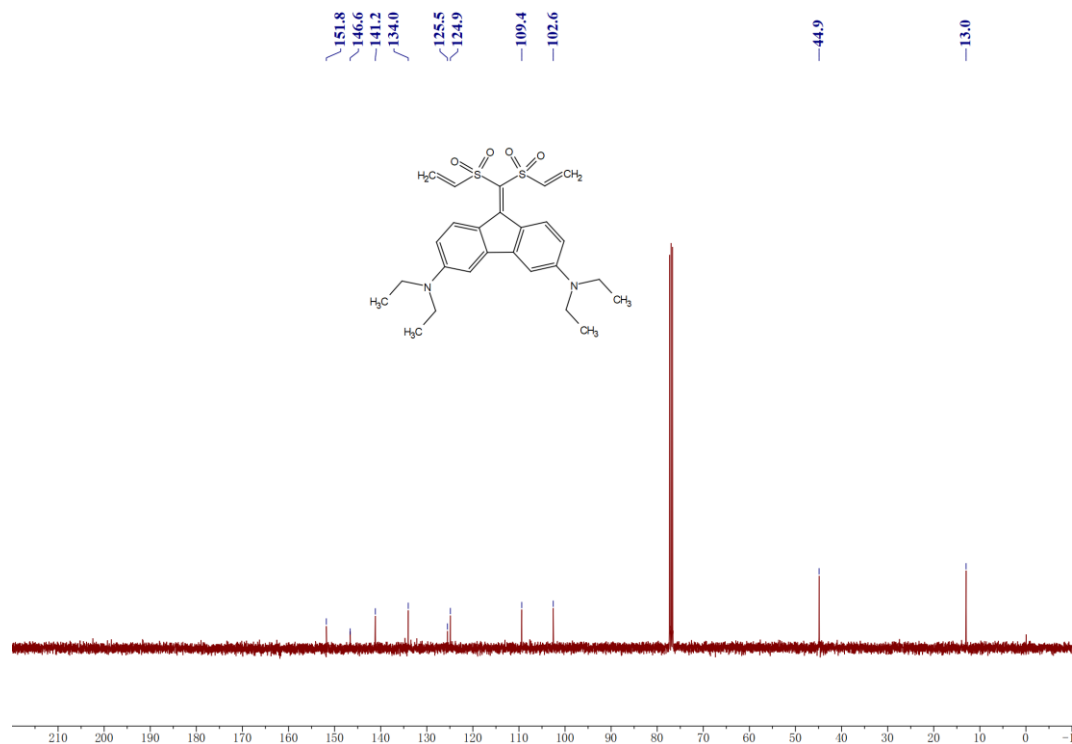


Figure S27. The <sup>13</sup>C NMR spectra of FE-VSM.

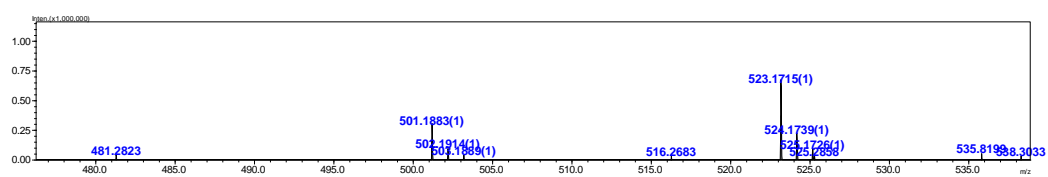


Figure S28. The HR-MS spectra of FE-VSM.

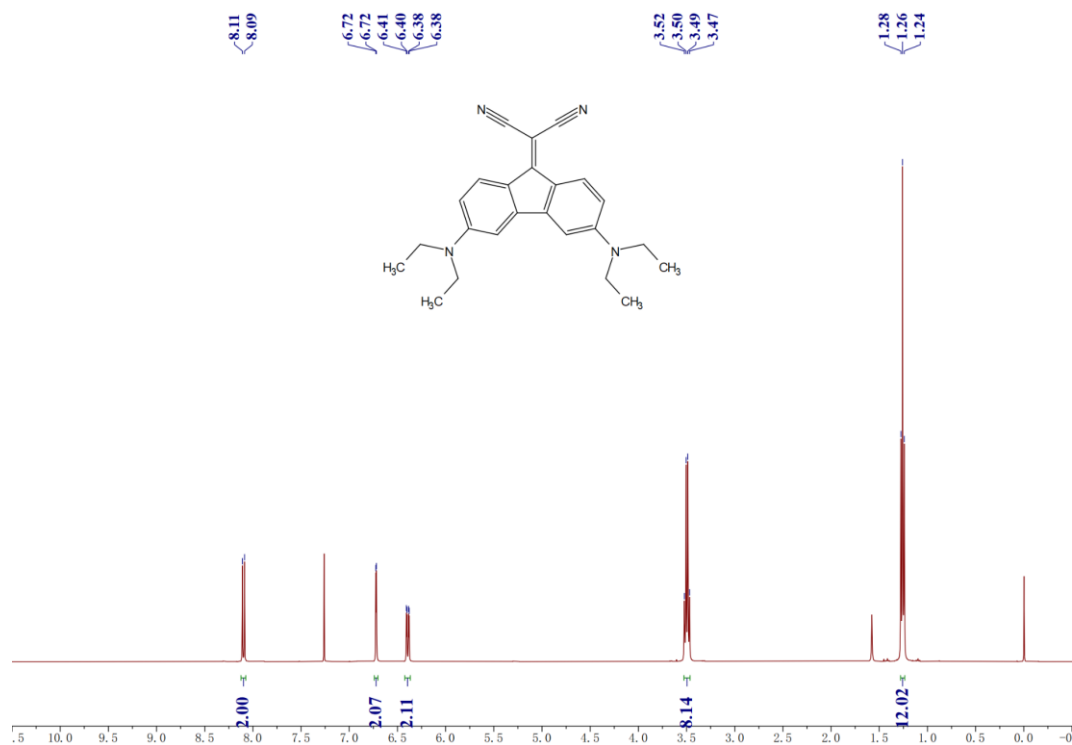


Figure S29. The <sup>1</sup>H NMR spectra of FE-MDN.

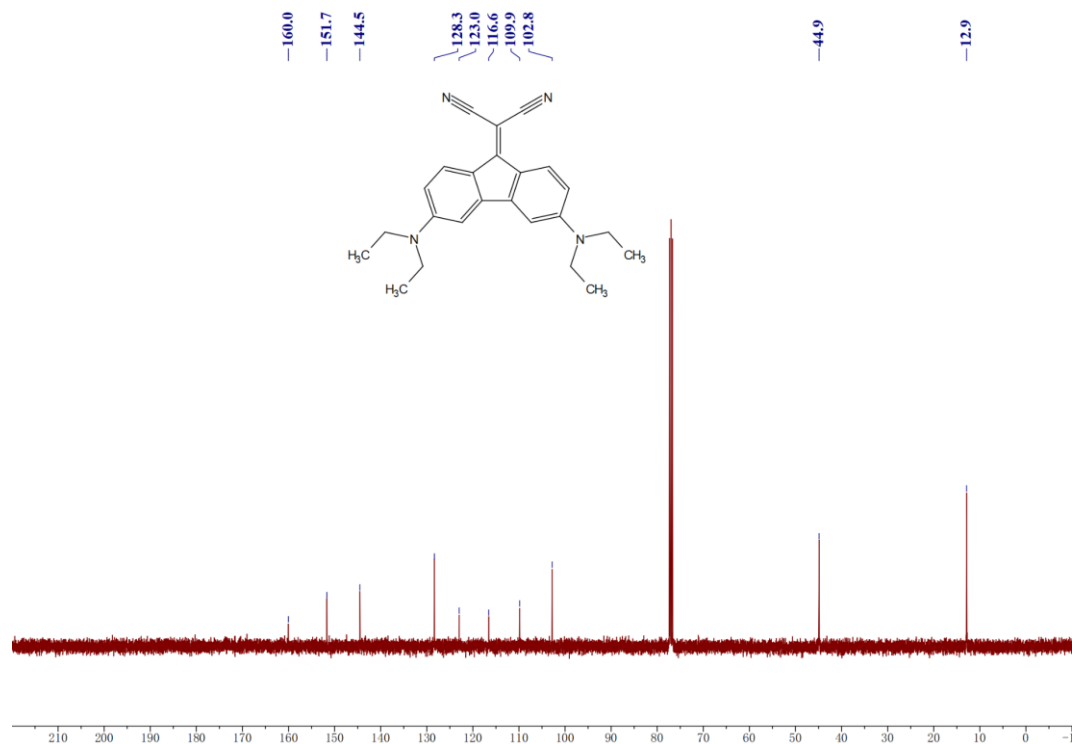


Figure S30. The <sup>13</sup>C NMR spectra of FE-MDN.

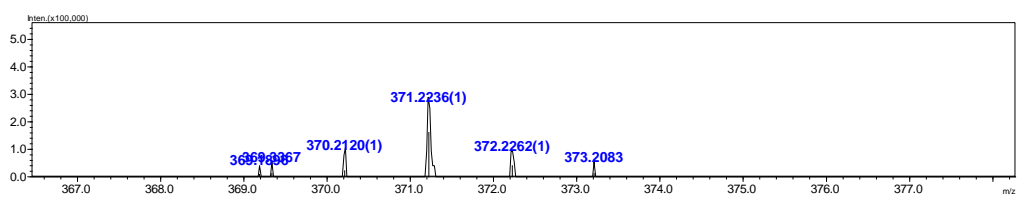


Figure S31. The HR-MS spectra of FE-MDN.

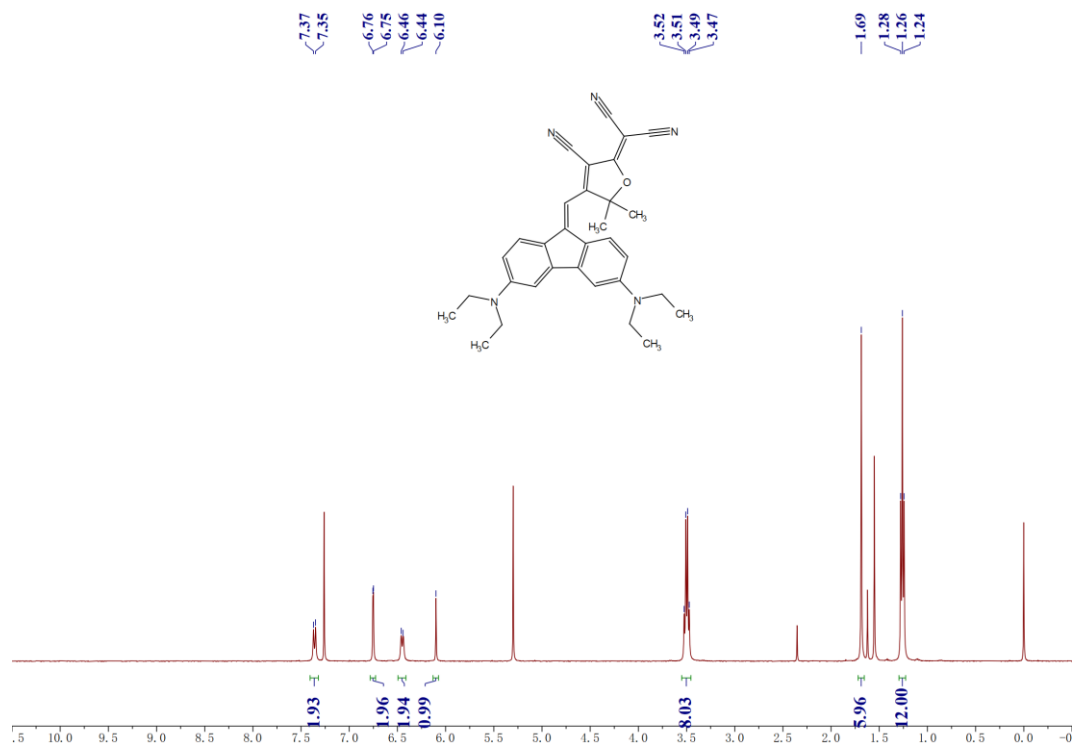


Figure S32. The <sup>1</sup>H NMR spectra of FE-TCF.

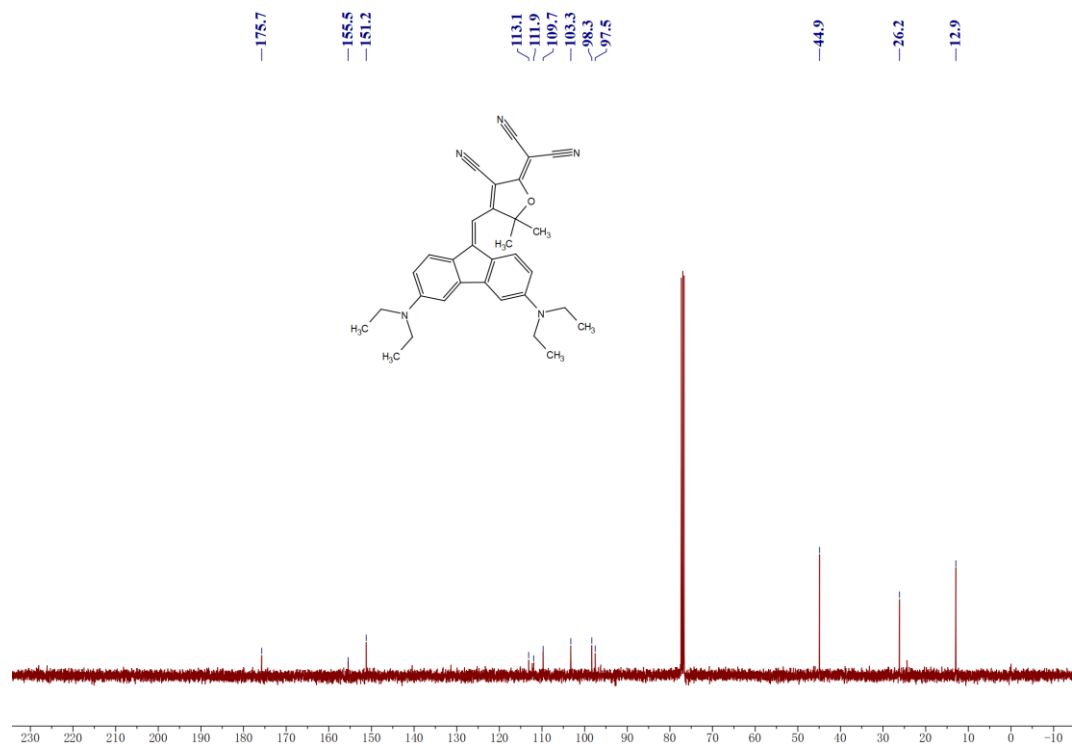


Figure S33. The <sup>13</sup>C NMR spectra of FE-TCF.

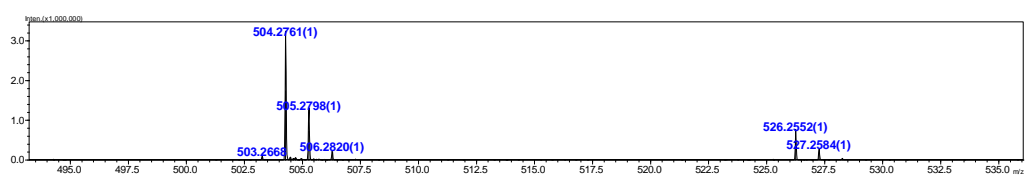




Figure S34. The  $^{13}\text{C}$  NMR spectra of FE-TCF.

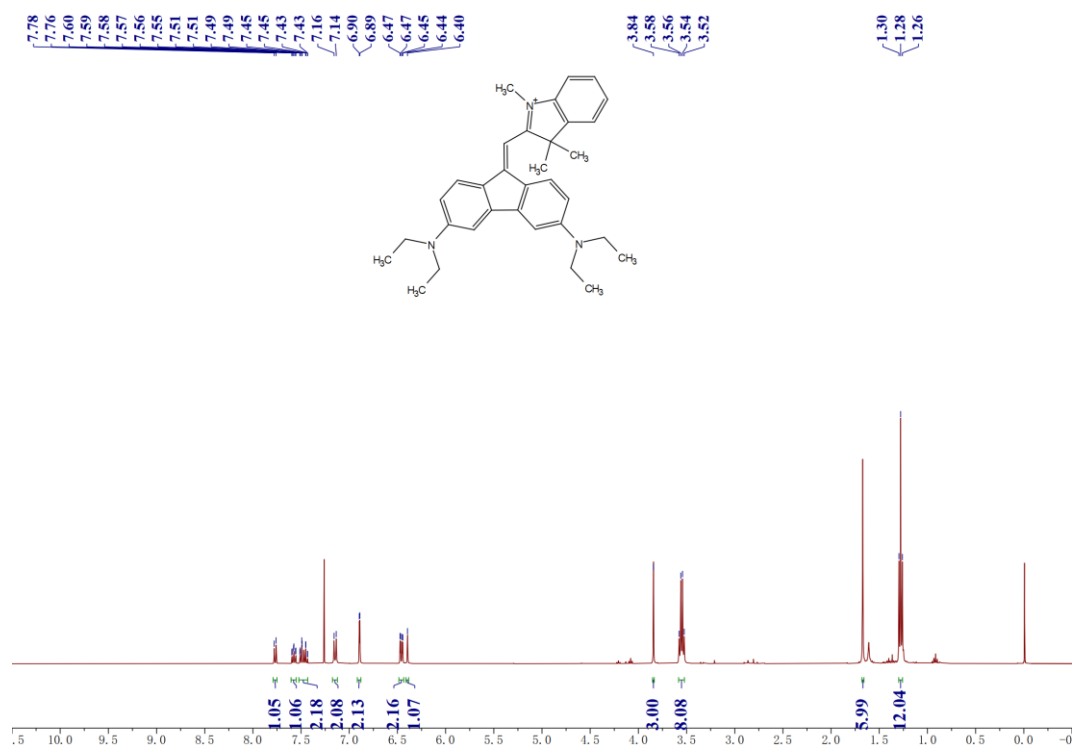


Figure S35. The  $^1\text{H}$  NMR spectra of FE-TMI.

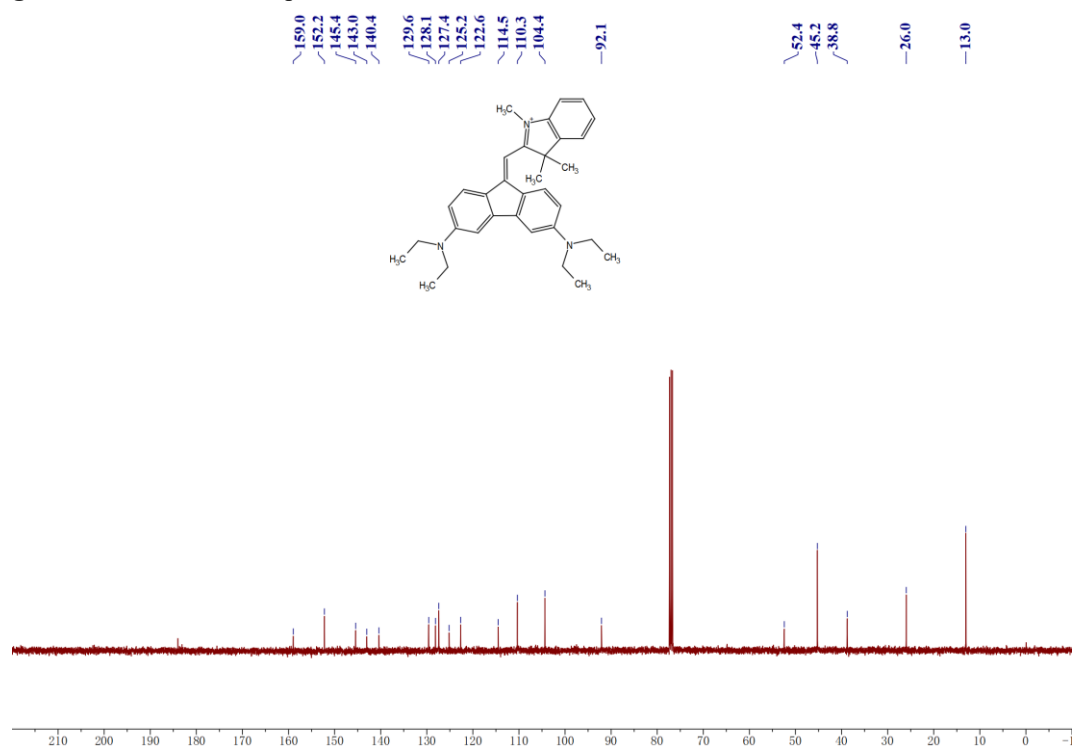


Figure S36. The  $^{13}\text{C}$  NMR spectra of FE-TMI.

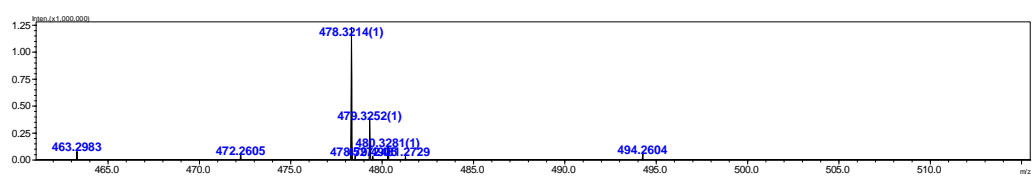


Figure S37. The HR-MS spectra of FE-TMI.

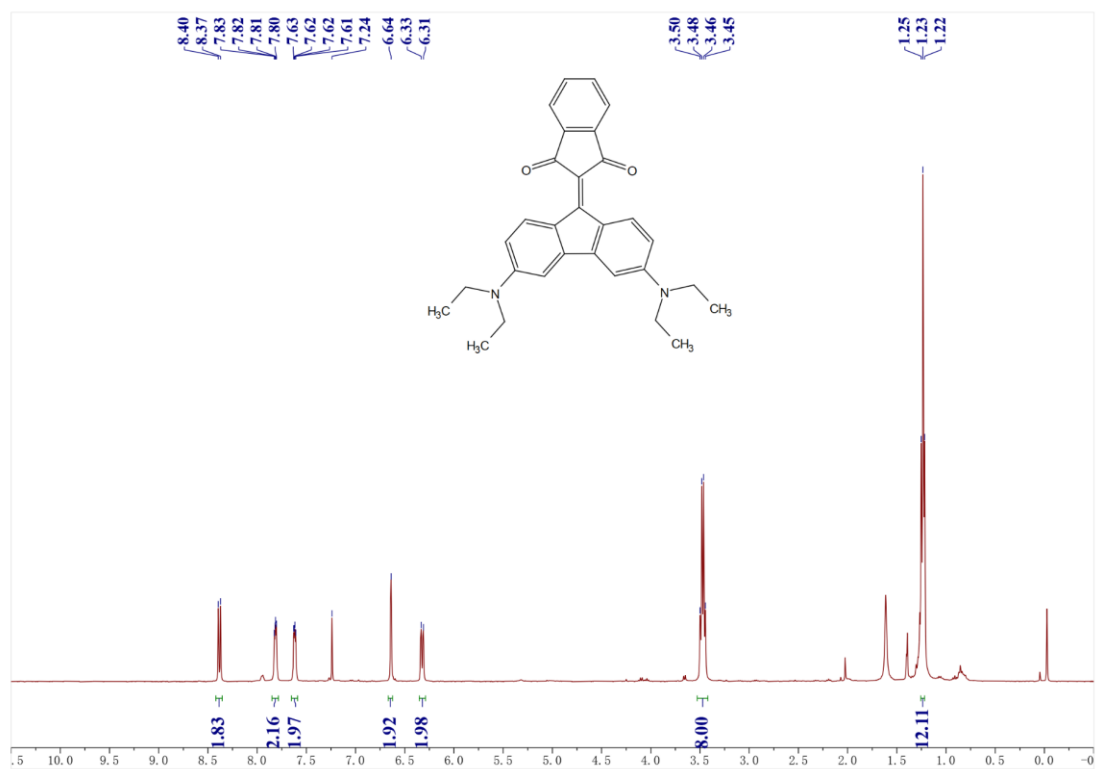


Figure S38 The <sup>1</sup>H NMR spectra of FE-ID

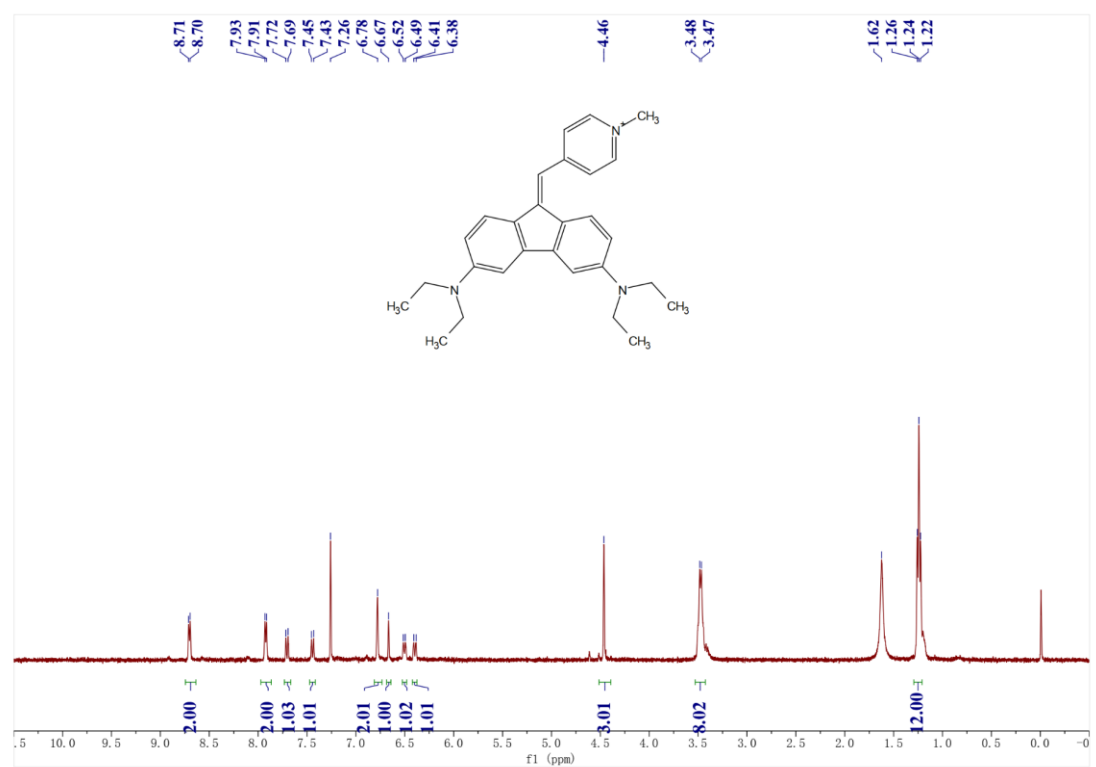


Figure S39. The <sup>1</sup>H NMR spectra of FE-MP.

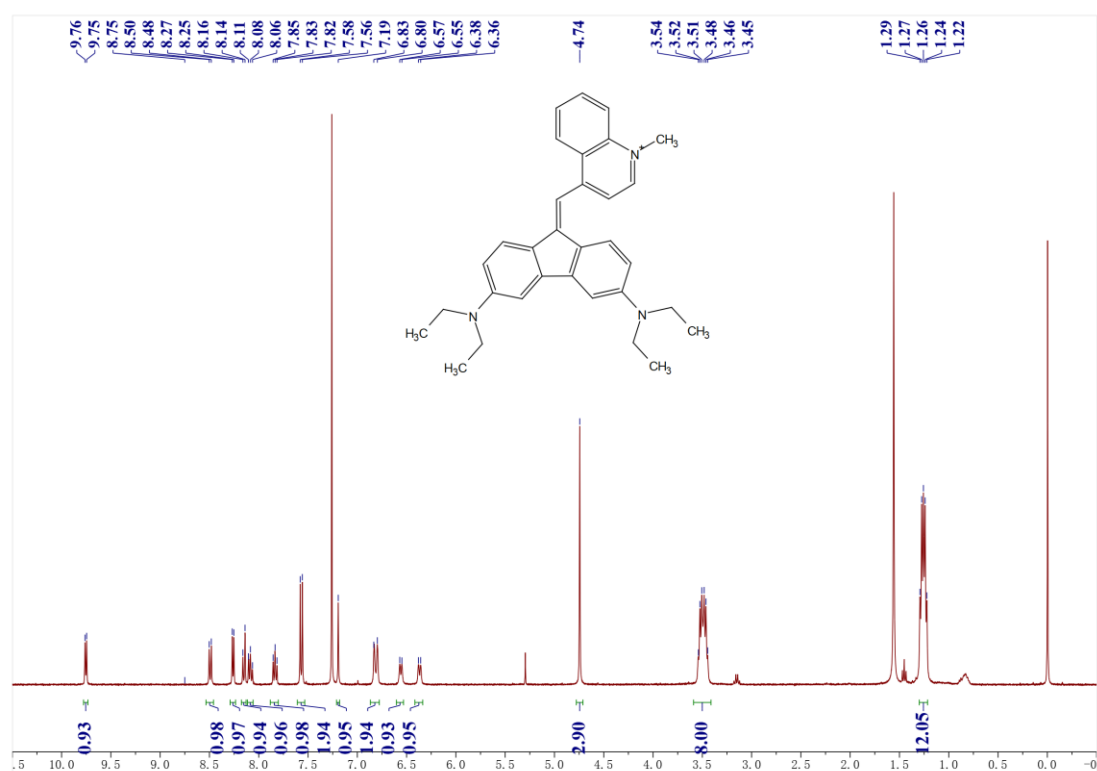


Figure S40. The <sup>1</sup>H NMR spectra of FE-MQ.

## REFERENCE

- [1] Y. Liu, X. Ran, D. Zhou, H. Zhang, Y. Chen, J. Xu, S. Chen, Q. Kong, X. Yu, K. Li, Novel Dibenzofulvene-Based NIR-II Emission Phototheranostic Agent with an 82.6% Photothermal Conversion Efficiency for Photothermal Therapy. *Adv. Funct. Mater.* **2023**, 23113653.
- [2] J. An, S. Tang, G. Hong, W. Chen, M. Chen, J. Song, Z. Li, X. Peng, F. Song, W. H. Zheng, An unexpected strategy to alleviate hypoxia limitation of photodynamic therapy by biotinylation of photosensitizers. *Nat. Commun.* **2022**, 13, 2225.
- [3] J. Zhuang, B. Wang, H. Chen, K. Zhang, N. Li, N. Zhao, B. Z. Tang, Efficient NIR-II Type-I AIE Photosensitizer for Mitochondria-Targeted Photodynamic Therapy through Synergistic Apoptosis–Ferroptosis. *ACS Nano* **2023**, 17, 9110-9125.
- [4] M. Li, Y. Shao, J. Kim, Z. Pu, X. Zhao, H. Huang, T. Xiong, Y. Kang, G. Li, K. Shao, J. Fan, J. Foley, J. Kim, X. Peng, Unimolecular Photodynamic O<sub>2</sub>-Economizer To Overcome Hypoxia Resistance in Phototherapeutics. *J. Am. Chem. Soc.* **2020**, 142, 5380–5388.
- [5] K. Teng, W. Chen, L. Niu, W. Fang, G. Cui, Q. Yang, BODIPY-Based Photodynamic Agents for Exclusively Generating Superoxide Radical over Singlet Oxygen. *Angew. Chem. Int. Ed.* **2021**, 60, 19912 – 19920.
- [6] Y. Xu, Y. Xie, Q. Wan, J. Tian, J. Liang, J. Zhou, M. Song, X. Zhou, M. Teng, Mechanism research of type I reactive oxygen species conversion based on molecular and aggregate levels for tumor photodynamic therapy. *Aggregate* **2024**, e612.
- [7] M. Zhao, Y. Zhang, J. Miao, H. Zhou, Y. Jiang, Y. Zhang, M. Miao, W. Chen, W. Xing, Q. Li, Q. Miao, An Activatable Phototheranostic Probe for Anti-hypoxic Type I Photodynamic- and Immuno-Therapy of Cancer. *Adv. Mater.* **2024**, 36, 2305243.

- [8] J. Tian, B. Li, F. Zhang, Z. Yao, W. Song, Y. Tang, Y. Ping, B. Liu, Activatable Type I Photosensitizer with Quenched Photosensitization Pre and Post Photodynamic Therapy. *Angew. Chem. Int. Ed.* **2023**, *62*, e202307288.